Am J Cancer Res 2026;16(2):721-740
www.ajcr.us /ISSN:2156-6976/ajcr0167622

Original Article

SLC7A5 serves as a potential therapeutic target for osteosarcoma: a comprehensive analysis based on bioinformatics and experimental validation

Ziliang Yu[1,2*], Feihu Chen[3*], Yixuan Li[1,2], Jiafeng He[1,2], Dagong Gao[1,2], Fei Xia[1,2], Haiping Zhang[1,2]

[1]Department of Orthopedic Surgery, Nantong First People's Hospital, Affiliated Hospital 2 of Nantong University, Nantong 226000, Jiangsu, China; [2]Department of Orthopedic Surgery, Nantong Hospital of Renji Hospital Affiliated to Shanghai Jiao Tong University School of Medicine, Nantong 226000, Jiangsu, China; [3]Department of Orthopedic Surgery, Xuyi People's Hospital, Huai'an 211700, Jiangsu, China. [*]Equal contributors.

Received July 22, 2025; Accepted February 25, 2026; Epub February 25, 2026; Published February 28, 2026

Abstract: This study aimed to investigate the role of solute carrier family 7 member 5 (SLC7A5) in osteosarcoma (OS) and its potential as a therapeutic target. Pan-cancer analysis revealed that SLC7A5 is significantly overexpressed in various tumor types, with particularly prominent upregulation in osteosarcoma. Using datasets from The Cancer Genome Atlas (TCGA), we found that high SLC7A5 expression was closely associated with poor patient prognosis, tumor multifocality, and metastatic progression. Based on SLC7A5-related genes, we constructed a prognostic risk score model using LASSO regression. This model effectively stratified patients by risk, revealing significant differences in survival outcomes between the high-risk and low-risk groups. In in vitro experiments, SLC7A5 overexpression significantly promoted the proliferation, migration, and invasion of osteosarcoma cells; conversely, silencing SLC7A5 not only inhibited these cellular behaviors but also induced apoptosis. Combining RNA sequencing with pathway enrichment analysis, we found that SLC7A5 regulates the phosphorylation levels of the mTOR pathway and its downstream target S6. In vivo experiments showed that SLC7A5 overexpression accelerated the growth of mouse xenograft tumors. Consistent with the in vitro functional assays, Ki-67 and phosphorylated mTOR levels were also elevated in tumor tissues, further validating the association between SLC7A5 and mTOR-mediated tumor progression.

Keywords: SLC7A5, osteosarcoma, immune infiltration, prognosis, IFN-γ response

Introduction

Osteosarcoma is a relatively common malignant bone tumor in young populations, and its incidence has been gradually increasing [1]. It generally originates from rapidly proliferating bone cells and exhibits high malignancy with a tendency for early metastasis, leading to poor patient prognosis [2, 3]. With the widespread use of immunotherapy and novel adjuvant chemotherapy regimens, the five-year survival rate of osteosarcoma patients has improved to some extent. However, the survival rate for patients with recurrent or metastatic osteosarcoma remains below 30% [4, 5]. Thus, exploring the underlying molecular mechanisms of osteosarcoma is of great significance for the development of new therapeutic strategies.

The bone microenvironment is a complex structural system composed of multiple cellular components and the extracellular matrix. The complex interactions between OS cells and the bone microenvironment significantly influence various tumor behaviors, including tumor development, metastasis, angiogenesis, therapeutic response, and pre-metastatic niche formation [6-8]. Within the microenvironment, immune cells play a crucial role in predicting the prognosis of OS. For instance, CD8+ T cells and natural killer (NK) cells possess anti-tumor capabilities, whereas myeloid-derived suppressor cells, M2-type macrophages, and regulatory T

https://doi.org/10.62347/WFPQ3511

(Treg) cells contribute to tumor progression [9-11]. Various cytokines and exosomes secreted by immune cells also play an indispensable regulatory role in the formation and progression of osteosarcoma [12, 13].

In osteosarcoma treatment, conventional chemotherapy and surgery remain the core approaches, but strategies combining immunotherapy with targeted therapy are gradually emerging as promising alternatives. Studies have not only highlighted the critical role of the tumor microenvironment and tumor suppressor gene inactivation in various cancers but also provided new directions for osteosarcoma therapy [14-18]. Mutations in tumor suppressor genes are relatively common molecular events across multiple cancer types, with inactivation of TP53 and RB1 genes being the most representative. Such mutations often accelerate tumor initiation and progression. In osteosarcoma, these genetic alterations may also exert similar pro-tumorigenic effects and significantly influence treatment outcomes [14]. Clinical studies have also focused on the combined use of immunotherapy and chemotherapy. Although such combinations did not significantly reduce recurrence rates in uterine leiomyosarcoma [15], these findings still offer valuable insights for osteosarcoma treatment, particularly regarding combination strategies. The roles of nutritional status and inflammatory responses in cancer therapy are increasingly recognized. Lower nutritional indices have been closely associated with poorer survival outcomes, a pattern observed across multiple tumor types, suggesting potential relevance in osteosarcoma treatment [16]. Sahin et al. found that an elevated neutrophil-to-eosinophil ratio closely correlates with significantly lower overall survival and progression-free survival [18]. This finding suggests that similar immune markers could help predict the immune microenvironment in osteosarcoma (OS) [17].

The proliferation and metastasis of tumor cells are highly dependent on the uptake of exogenous amino acids [19, 20]. Solute carrier family 7 member 5 (SLC7A5), also known as large neutral amino acid transporter 1, serves as a transmembrane transporter for amino acids [21]. Existing evidence indicates that SLC7A5 is overexpressed in various malignant tumors and exerts pro-tumor effects through its transport activity. Specifically, SLC7A5-mediated glutamine influx, along with the subsequent activation of the mTORC1 signaling pathway, synergistically upregulates the expression of the transcription factor c-Myc, thereby driving malignant tumor progression [22-24]. The increased expression of SLC7A5 has also been associated with unfavorable prognoses for patients [25-27]. Increased expression of SLC7A5 enhances the activation of $CD4^+$ T cells, thereby stimulating immune responses [28]. Broer et al. found that 143B OS cells express a group of glutamine transporter proteins, including SLC7A5 [29]. Investigate the biological function of SLC7A5 in OS may unveil its potential use as a new tumor biomarker and therapeutic target.

In this study, we investigated the relationship between SLC7A5 expression and clinical characteristics, prognosis, and immune status in OS was investigated through an in-depth analysis of The Cancer Genome Atlas (TCGA) database. Additionally, it was unveiled that SLC7A5 promotes the proliferation of OS cells both *in vitro* and *in vivo*, suggesting that SLC7A5 has the potential to serve as a valuable clinical biomarker and target for advanced therapy in OS.

Materials and methods

Public dataset acquisition and preprocessing

In the pursuit of evaluating SLC7A5 expression among patients with cancer, the mRNA expression profiles and the corresponding clinical information were obtained from the TCGA pancancer cohort (https://portal.gdc.cancer.gov/). The amalgamation of multiple Gene Expression Omnibus cohorts, specifically GSE19276 [30], GSE87624 [31], and GSE99671 [32], was performed, and the mitigation of batch effects was undertaken through the application of the combat algorithm housed within the 'sva' package (Version 3.52.0). To ensure data consistency and comparability across samples, we performed rigorous standardization of the raw data using the transcripts per million (TPM) method for normalization. This step was crucial for achieving accurate and consistent comparisons between samples.

Analysis of prognosis and the clinicopathological correlation

The cutoff value for discerning SLC7A5 expression in sarcoma tissues as either high or low

was determined based on the median expression level. The analysis of the correlation between SLC7A5 expression and various clinicopathological features, such as sex, age, tumor multifocality, residual tumor, tumor necrosis, tumor depth, and metastasis, was performed using the corresponding methodologies. Overall survival curves were generated using data from the TCGA-Sarcoma (SARC) dataset and Kaplan-Meier Plotter (https://kmplot.com/analysis/).

Screening co-expressed genes and differentially expressed genes (DEGs)

The co-expressed genes of SLC7A5 were determined using Spearman's correlation coefficient using the TCGA-SARC dataset. Subsequently, the R package 'Deseq2' was employed to identify DEGs between the groups characterized by high and low SLC7A5 expression. The filtering criteria for this analysis were set at |log2 fold change (FC)| > 1 and false discovery rate (FDR) < 0.05.

Functional enrichment analysis

Gene Ontology (GO) enrichment and Kyoto Encyclopedia of Genes and Genomes (KEGG) pathway analyses were employed to investigate potential biological processes (BPs), cellular components (CCs), and molecular functions (MFs) associated with DEGs between SLC7A5 high- and low-expression groups. A statistically significant threshold was defined as an FDR q value < 0.05. The significantly enriched pathways were visualized using bubble plots.

Establishment of an SLC7A5-derived prognostic gene model

The R package 'glmnet' was used to identify the top 30 DEGs that were upregulated in the SLC7A5 high-expression group. These DEGs were then subjected to a least absolute shrinkage and selection operator (LASSO) penalized Cox regression analysis to construct a prognostic model by selecting the most relevant genes from the initial pool of 30 candidate genes. The normalized expression levels of the candidate DEGs and the corresponding survival data, including time and status, were used as the independent and dependent variables, respectively, for the LASSO regression. A 10-fold cross-validation was performed to determine the penalty parameter (λ) based on the minimum criteria. Using the expression levels of the DEGs and their corresponding coefficients, a risk score was calculated for each patient. The following formula was used to calculate the risk score: risk score = (SLC7A5 × 0.1146814) + [ceramide synthase 1 (CERS1) × 0.04358834] - [tumor necrosis factor receptor-associated factor 3-interacting protein 3 (TRAF3IP3) × 0.12706772] + [regulatory factor X6 (RFX6) × 0.02177245] + [RANBP2 like and GRIP domain containing 1 (RGPD1) × 1.18127866] + [CUB and Sushi multiple domains 3 (CSMD3) × 0.03530255]. The median risk score was used to divide the patients into low- and high-risk cohorts. Kaplan-Meier analysis was conducted to compare the overall survival between these risk groups. To assess the diagnostic efficacy of the risk model, a receiver operating characteristic (ROC) curve was generated using the R packages 'survival', 'survminer', and 'time-ROC'.

Immune infiltration and correlation analyses

An immune infiltration analysis was conducted using the single-sample Gene Set Enrichment Analysis (ssGSEA) algorithm. This approach allowed the exploration of the potential connection between SLC7A5 and the tumor immune microenvironment. The ssGSEA algorithm is capable of quantifying 24 known tumor-infiltrating lymphocyte cell types based on the provided expression matrix.

Cell culture

The osteoblast cells and OS cell lines MG-63, HOS, and U2-OS were obtained from BeNa Culture Collection, Beijing Beina Chunglian Institute of Biotechnology. Cell cultures were maintained in DMEM medium (Cytiva; cat. no. SH30022.02), supplemented with 10% fetal bovine serum (Corning; cat. no. 35-081-CV) and 1% penicillin-streptomycin (Solarbio; cat. no. P1400). The cells were incubated at 37°C and 5% CO_2. Subculturing was carried out when cell density reached 75-85% confluence.

Transfection

Lentiviruses containing an overexpression or an interfering sequence for SLC7A5 were procured from Shanghai Hanheng Biotech Co.,

Ltd. OS cells were transfected with either lenti-oeSLC7A5, lenti-shSLC7A5 or relative negative control, and polybrene (8 μg/ml) was introduced to augment the efficiency of infection. A total of 72 h after infection, cells were collected for further assays.

RNA isolation and reverse transcription-quantitative PCR (RT-qPCR)

Cells were subjected to total RNA extraction using the RNA extraction kit (Solarbio; cat. no. R1200). The isolated RNA was subsequently reverse transcribed into cDNAs with M-MLV reverse transcriptase (Promega; cat. no. M1701). The primer sequences employed were as follows: SLC7A5-forward (F), 5'-GCATCGGCTTCACCATCATC-3'; SLC7A5-reverse (R), 5'-ACCACCTGCATGAGCTTCTGAC-3'; GAPDH-F, 5'-GACCTGACCTGCCGTCTAG-3'; GAPDH-R, 5'-AGGAGTGGG TGTCGCTGT-3'. Quantitative PCR was performed using an ABI 7500 system, and the relative mRNA expression levels of SLC7A5 were quantified using the $2^{-\Delta\Delta Cq}$ method.

Western blotting

Cellular protein was isolated from each group utilizing a radioimmunoprecipitation assay lysate (Beyotime; cat. no. P0013C). The concentration of proteins was determined through the bicinchoninic acid method (Beyotime; cat. no. P0011). Protein samples (50 μg each) were subjected to polyacrylamide gel electrophoresis and then transferred to a polyvinylidene fluoride membrane. The membrane was blocked with 5% skimmed milk for 1 h at room temperature. After blocking, it was incubated overnight with the primary antibody for SLC7A5 (ProteinTech; cat. no. 28670-1-AP; 1:5000), mTOR (Abclonal; cat. no. A2445; 1:2000), Phospho-mTOR (Abclonal; cat. no. AP0094; 1:1000), S6 (Abclonal; cat. no. A6058; 1:1000), Phospho-S6 (Abclonal; cat. no. AP1328; 1:20000) and β-actin (ProteinTech; cat. no. 81115-1-RR; 1:5000). The next day, the secondary antibody (ProteinTech; cat. no. SA00001-2; 1:2000) was added and incubated for 1 h at room temperature for development.

Cell Counting Kit-8 (CCK-8) assay

Cell proliferation in MG63 and HOS cells was assessed both before transfection and on days 1, 2, 3, and 4 following transfections, utilizing a CCK-8 assay kit (Absin, cat. no. abs50003). The cells were cultured with the CCK-8 reagent for 4 h, after which the optical density was measured at 450 nm employing a microplate reader (Tecan; Infinite F50).

Cell apoptosis detection

For cell apoptosis analysis, the Annexin V-FITC apoptosis detection kit (Absin; cat. no. abs50001) was employed. The staining procedure followed the manufacturer's guidelines. In brief, cells were double-stained with 5 μl Annexin V-FITC and 10 μl propidium iodide in each tube. After gentle vortexing, the samples were incubated in the dark at room temperature for 15 min. Subsequently, the samples were injected and examined using a flow cytometer (Beckman; CytoFLEX S).

Wound scratch assay

After trypsinization and centrifugation, cells were seeded at a predetermined density into 6-well plates containing complete culture medium. Following overnight adhesion, three parallel and vertical scratches were made perpendicular to the plate using a 1 mL pipette tip. Images of the initial scratch morphology were captured (0 hours). After 24 hours of culture, images were taken at the same positions. Cell migration ability was evaluated by measuring the changes in scratch width.

Transwell assay

Transfected cells were trypsinized, resuspended in serum-free medium, and adjusted to a density of 1×10^5 cells/mL. The upper surface of the Transwell membrane was coated with Matrigel (BD Biosciences; cat. no. 356234; 1:8 dilution) and incubated at 37°C for 30 min to allow gelation. A total of 100 μL of the cell suspension, containing 1×10^4 cells, was carefully seeded into the upper chamber, while the lower chamber was filled with complete medium. After overnight incubation, fixation, staining, and analysis were performed following the migration assay procedure described above.

RNA-sequencing

We collected transfected MG63 and HOS cells (2×10^6 cells) and extracted total RNA using a

TRIzol kit. RNA sequencing was performed by Shanghai Meiji Biomedical Technology Co., Ltd. on the Illumina NovaSeq 6000 platform. Differentially expressed genes (DEGs) were identified using the criteria of $P < 0.05$ and absolute $\log_2$ fold change > 1.

Animal experiments

Sixteen 4-week-old male BALB/c nude mice, weighing 18-22 g, were purchased from Shanghai Lingshang Biotechnology Co., Ltd. and acclimatized for one week after arrival. Each mouse was subcutaneously inoculated with 2×10^6 MG63 cells into the right axillary region. Tumor volume was measured every 5 days starting from day 10 post-inoculation, calculated using the formula: tumor volume = length × width^2/2. All mice were housed under specific pathogen-free (SPF) conditions, with controlled temperature, humidity, light-dark cycles, and free access to food and water. Due to the minor trauma associated with the procedure, no analgesics were administered during the experiment, and no symptoms such as trembling or huddling were observed in the mice. Their health status was monitored daily. All mice survived until the predetermined experimental endpoint (day 40) and were euthanized by cervical dislocation under pentobarbital sodium anesthesia (30-90 mg/kg). No criteria for humane endpoints (e.g., body weight loss exceeding 20%, tumor ulceration, or severe distress) were observed during the experiment. Death was confirmed by cessation of heartbeat and respiration. All animal carcasses were centrally processed by the Laboratory Animal Center according to institutional hazardous waste disposal protocols. All animal procedures were approved by the Nantong University Laboratory Animal Ethics Committee (NTULAC, No. P20230228-093), and the study was conducted in accordance with the ARRIVE guidelines and NIH standards for tumor burden control.

Immunohistochemistry

The fresh tissue was soaked in 4% paraformaldehyde for 24 h, cut to a suitable size, and completely soaked in paraffin solution. After the paraffin solidified, the wax block was cut into 4 μm slices, baked, and immobilized on the slide to form a paraffin section. The slices were then dewaxed and rehydrated with xylene and a series of graded alcohols, followed by EDTA antigen retrieval, 10 min of incubation with 3% H_2O_2 at room temperature after two PBS rinsings, and 30 min of blocking with 5% silk milk after three PBS washing. The section was incubated at 4°C overnight with primary antibodies (anti-p-mTOR (Abclonal; cat. no. AP0094; 1:200) and ki-67 (Abclonal; cat. no. A2094; 1:800)). After rinsing with PBS three times, the secondary antibody (Abclonal; cat. no. AS014; 1:100) was introduced and incubated at 37°C for 30 min. Then DAB (ServiceBio; cat. no. G1212) was employed for color development and hematoxylin (ServiceBio; cat. no. G1004) was for re-staining. the section was dehydrated, transparent, and sealed with neutral resin. The slide was observed and photographed under an optical microscope (Nikon; Ci-S).

Statistical analysis

We constructed a LASSO regression model and evaluated its predictive performance using ROC curves. The relationship between gene expression and patient prognosis was analyzed using Kaplan-Meier survival curves and the Log-rank test, implemented with the R packages survival (3.3-0) and survminer (0.4.8). Immune infiltration levels were quantified using single-sample gene set enrichment analysis (ssGSEA). Cellular experimental data were organized and analyzed using GraphPad Prism 8.0. Each experiment was independently repeated at least three times, and results are presented as mean ± standard deviation (mean ± SD). Statistical analysis methods were selected according to the experimental design: comparisons between two groups were performed using unpaired t-tests, comparisons among multiple groups were performed using one-way ANOVA, and experiments involving multiple factors were analyzed using repeated measures ANOVA. A value of $P < 0.05$ was considered statistically significant.

Results

Analysis of SLC7A5 overexpression in sarcoma and OS

The investigation commenced with an extensive analysis of SLC7A5 mRNA expression across various cancer types using TCGA datasets. Within the cohort of 33 cancer types, the expression of SLC7A5 showed distinct pat-

terns. SLC7A5 exhibited a substantial upregulation in several cancers, including breast invasive carcinoma, cervical and endocervical carcinoma, cholangiocarcinoma, colon adenocarcinoma, esophageal carcinoma, head and neck squamous cell carcinoma, liver hepatocellular carcinoma, lung adenocarcinoma, lung squamous cell carcinoma, pheochromocytoma and paraganglioma, rectum adenocarcinoma, stomach adenocarcinoma, thyroid carcinoma and uterine corpus endometrial carcinoma (**Figure 1A**). In three specific cancer types: Kidney chromophobe, kidney renal papillary cell carcinoma and prostate adenocarcinoma, a slight downregulation trend in SLC7A5 expression was observed.

To further verify whether SLC7A5 is aberrantly expressed in osteosarcoma, we additionally analyzed data from the GEO database. By analyzing the GSE19276 dataset comprising 23 OS samples and five non-malignant bone samples, GSE87624 consisting of 44 OS samples and five normal bone samples and GSE99671 encompassing 18 tumoral bone samples and 18 non-tumoral paired samples, significantly elevated expression of SLC7A5 in OS tissues compared with the non-tumor bone tissues were consistently observed (**Figure 1B**). Following this, patients with sarcoma were stratified into two cohorts based on the median expression level of SLC7A5: i) SLC7A5 high (top 50%); and ii) SLC7A5 low (bottom 50%). The association between SLC7A5 expression and various clinical characteristics was subsequently investigated (**Table 1**). The expression of SLC7A5 in sarcoma samples with tumor multifocality was significantly higher (**Figure 1C**), and a similar trend was observed in samples with metastasis (**Figure 1D**). Additionally, a comparison of survival curves revealed that a high mRNA level of the SLC7A5 gene was associated with poorer overall survival in patients with sarcoma [**Figure 1E**; hazard ratio (HR), 1.5; P = 0.0001].

Identification of SLC7A5-related genes in TCGA-SARC

The development of cancer is the consequence of the co-regulation of numerous genes. Based on the median expression levels of SLC7A5 in TCGA-SARC cohorts, samples were categorized into two groups: i) High SLC7A5 group; and ii) low SLC7A5 group, each comprising 132 samples. Using the DESeq2 method, DEGs were identified applying the criteria of |log2FC| > 1 and FDR < 0.05. A total of 479 downregulated genes and 635 upregulated genes were selected and presented in **Figure 2A**. Ranked by FC, **Figure 2B** and Table S1 display the top 10 upregulated genes and top 10 downregulated genes, respectively. To evaluate the co-expression patterns with SLC7A5, Spearman's correlation analysis was conducted, and several genes were identified, although the correlation coefficients were not modest. **Figure 2C** and Table S2 illustrate the top seven positively correlated genes and the top seven negatively correlated genes, respectively. The results showed that the genes positively correlated with the expression of SLC7A5 were PSAT1, RELT, RCC2, AUNIP, HMGB3, TUBA1C, and TPM3, whereas the expression of THRB, CPO, NENF, METTL7A, PDE1B, AOC3, and ACBD4 was negatively correlated with SLC7A5. These co-expressed genes may have mutual mechanisms of action working together in the progression of OS.

Establishment of an SLC7A5-derived genomic model for sarcoma prognosis

SLC7A5 expression in the TCGA database can predict survival outcomes in osteosarcoma patients. However, due to the relatively low area under the curve (AUC) (Figure S1), the time-dependent ROC curve for SLC7A5 alone has limitations. To more accurately identify prognostic factors, the top 30 upregulated genes in SLC7A5-high sarcoma samples were used as input for a random survival forest analysis (**Figure 3A**). The relative importance of these prognostic genes was calculated and ranked. Based on their importance values, six genes-SLC7A5, CERS1, TRAF3IP3, RFX6, RGPD1, and CSMD3-were selected (**Figure 3B**), and the risk score was calculated as follows: Risk score = (SLC7A5 × 0.1146814) + (CERS1 × 0.04358834) - (TRAF3IP3 × 0.12706772) + (RFX6 × 0.02177245) + (RGPD1 × 1.18127866) + (CSMD3 × 0.03530255). Using the mean risk score, OS patients were stratified into two subgroups: i) high-risk and ii) low-risk. Although only SLC7A5 and TRAF3IP3 were independent survival-related factors (**Figure 3C-G**), the combination of these six genes significantly stratified patients according to overall survival, as indicated by a log-rank *P* value of 0.00016 (**Figure 3H**). ROC curve analysis confirmed that

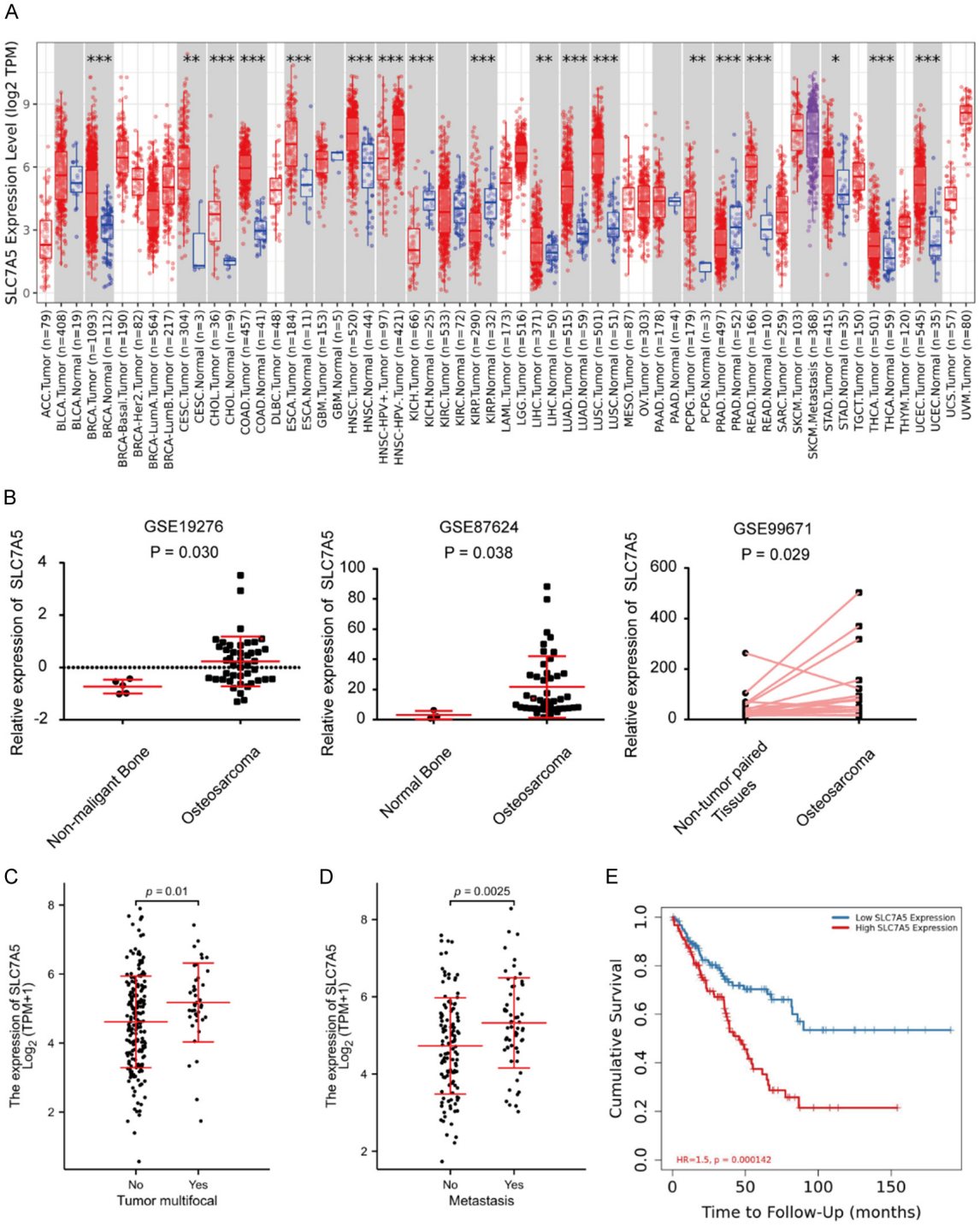

Figure 1. High expression of SLC7A5 in multiple cancers, including OS, correlates with poor survival in sarcoma. A. Determination of SLC7A5 expression in multiple tumors and corresponding normal tissues from the TCGA database (red, tumor group; blue, normal group; purple, metastatic tumor group; *P<0.05). B. OE of SLC7A5 in OS tissues and cells compared with control confirmed in GSE19276, GSE87624, and GSE99671 datasets. C. OE of SLC7A5 in multifocal sarcomas compared with non-multifocal sarcomas in TCGA-SARC cohorts. D. OE of SLC7A5 in metastatic sarcomas compared with non-metastatic sarcomas in TCGA-SARC cohorts. E. Kaplan-Meier survival curves show the correlation between overall survival and SLC7A5 expression. SLC7A5, solute carrier family 7 member 5; TCGA, The Cancer Genome Atlas; SARC, sarcoma; OE, overexpression; OS, osteosarcoma.

Table 1. Correlation among SLC7A5 expression and clinical characteristics of patients with sarcoma according to the TCGA database

Characteristics	SLC7A5 expression		*P* value	Statistic	Method
	Low	High			
n	131	132			
Gender, n (%)			0.2416	1.3713	Chi-square
Female	67 (25.5%)	77 (29.3%)			
Male	64 (24.3%)	55 (20.9%)			
Age, n (%)			0.9514	0.0037	Chi-square
≤ 60	65 (24.7%)	65 (24.7%)			
> 60	66 (25.1%)	67 (25.5%)			
Tumor multifocal, n (%)			0.0042*	8.1777	Chi-square
No	109 (45.6%)	90 (37.7%)			
Yes	12 (5%)	28 (11.7%)			
Residual tumor, n (%)			0.7336	0.6197	Yates's correction
R0	79 (33.6%)	78 (33.2%)			
R1	38 (16.2%)	31 (13.2%)			
R2	4 (1.7%)	5 (2.1%)			
Tumor necrosis, n (%)			0.1491	5.330	Chi-square
No necrosis	35 (19.1%)	36 (19.7%)			
Focal necrosis	19 (10.4%)	19 (10.4%)			
Moderate necrosis	25 (13.7%)	37 (20.2%)			
Extensive necrosis	2 (1.1%)	10 (5.5%)			
Tumor depth, n (%)			0.2406	1.377	Chi-square
Superficial	13 (6.2%)	8 (3.8%)			
Deep	91 (43.5%)	97 (46.4%)			
Metastasis, n (%)			0.0038*	8.3782	Chi-square
No	62 (34.6%)	58 (32.4%)			
Yes	17 (9.5%)	42 (23.5%)			

*P<0.05.

this SLC7A5-based prognostic model has strong potential for predicting patient outcomes (**Figure 3I**).

SLC7A5-associated immune infiltration landscape in sarcoma

We performed KEGG and GO enrichment analysis using the upregulated and downregulated differentially expressed genes (DEGs) as input. Through this analysis, we were able to identify activated and inactivated pathways associated with SLC7A5. The top four pathways with the lowest *p*-values in the BP, CC, MF, and KEGG categories are shown in **Figure 4A** and **4B**, with detailed information provided in Table S3. Notably, in the SLC7A5 high-expression group, both cytokine activity and cytokine-cytokine receptor interaction were identified as activated pathways, suggesting that SLC7A5 may play an important role in regulating the tumor microenvironment.

Furthermore, a GSEA was conducted to further confirm the functional implications of SLC7A5. The analysis revealed the activation of several pathways, including the CD8-T cell receptor (TCR) downstream pathway, interleukin 10 signaling, hedgehog signaling pathway, antigen processing and presentation, PD-1 signaling, NK cell-mediated cytotoxicity, interactions of NK cells in pancreatic cancer, cancer immunotherapy by PD1 blockade, and TCR signaling pathway. The corresponding normalized enrichment score, *P*-value, and FDR are presented in **Figure 4C** and Table S4.

Liang et al. found that there was significant immune cell infiltration in the adjacent tissues of osteosarcoma (OS). This infiltration formed a

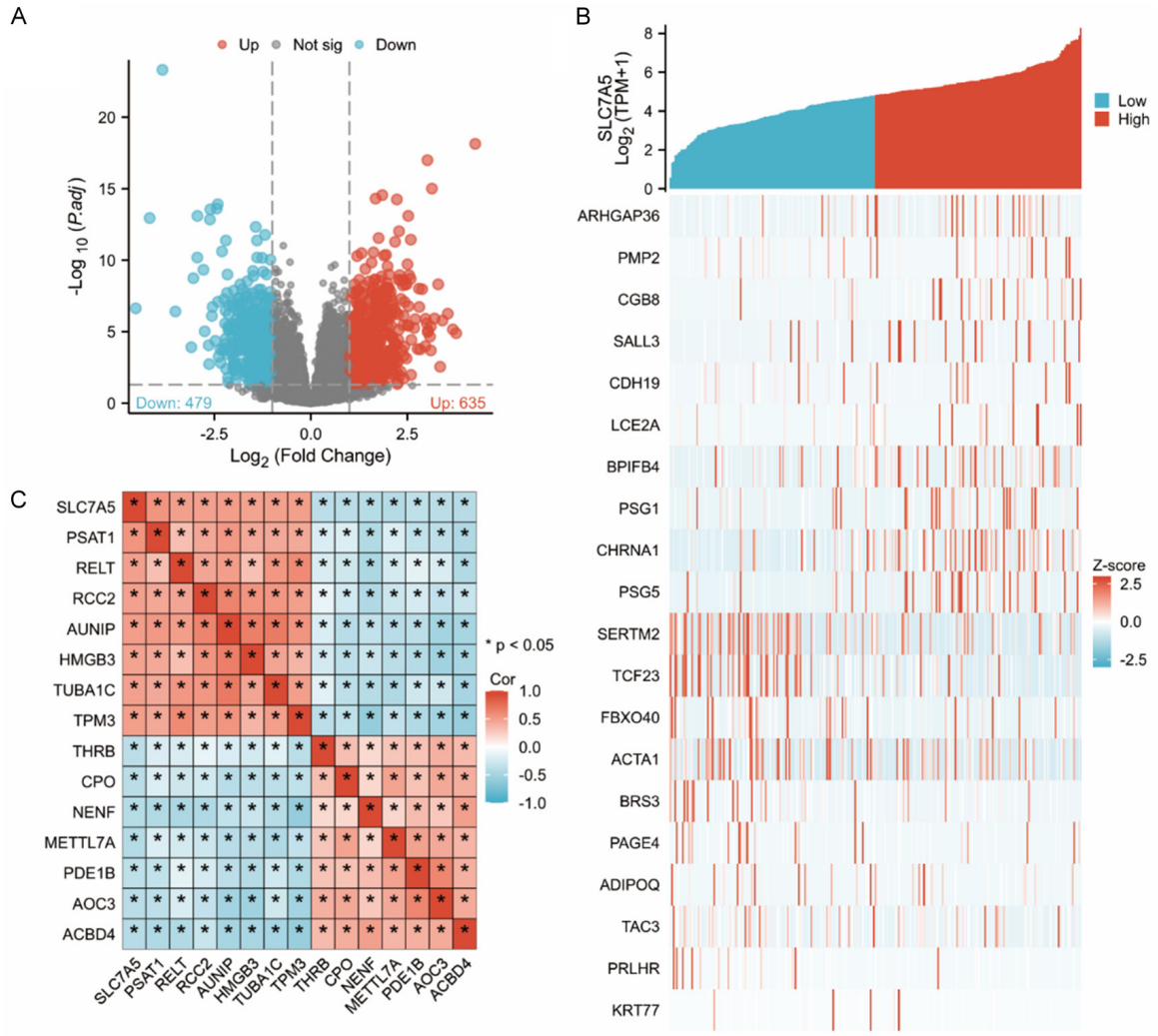

Figure 2. Identification of differentially expressed genes associated with SLC7A5 expression in TCGA-SARC cohorts. A. Volcano plots show upregulated and downregulated genes between SLC7A5-high and SLC7A5-low sarcoma samples. B. The heatmap illustrates the top 10 upregulated and downregulated genes. C. The heatmap shows the top seven positively correlated genes and the top seven negatively correlated genes from Spearman's correlation analysis. SLC7A5, solute carrier family 7 member 5; TCGA, The Cancer Genome Atlas; SARC, sarcoma.

complex immune microenvironment, which might promote the proliferation and survival of tumor cells within the bone under immunosuppressive conditions [33, 34]. To analyze the immune infiltration characteristics associated with SLC7A5 in sarcoma, we applied single-sample gene set enrichment analysis (ssGSEA) to evaluate the infiltration levels of different immune cell subsets. Through this approach, we systematically compared immune cell infiltration patterns across different sarcoma types in relation to SLC7A5 expression levels. Sarcoma cases with high SLC7A5 expression showed increased infiltration of various immune cells, including T helper (Th) 2 cells, macrophages, neutrophils, TFH cells, Tregs, and NK CD56dim cells (Figure S2A). These immune cell types are generally known to have immune-suppressing effects during tumorigenesis. Conversely, there was a negative correlation between SLC7A5 expression and infiltration of NK cells, plasmacytoid dendritic cells (DCs), mast cells, TGD cells, and DCs (Figure S2B). Most of these cell types are actively involved in the processes of antigen presentation, tumor recognition, and elimination. Spearman's correlation analysis further confirmed the correlation between SLC7A5 and dysregulated immune cells in each sample of TCGA-SARC cohorts (Figure S2C), providing additional support for the immune-suppressing role of SLC7A5 in the sarcoma microenvironment.

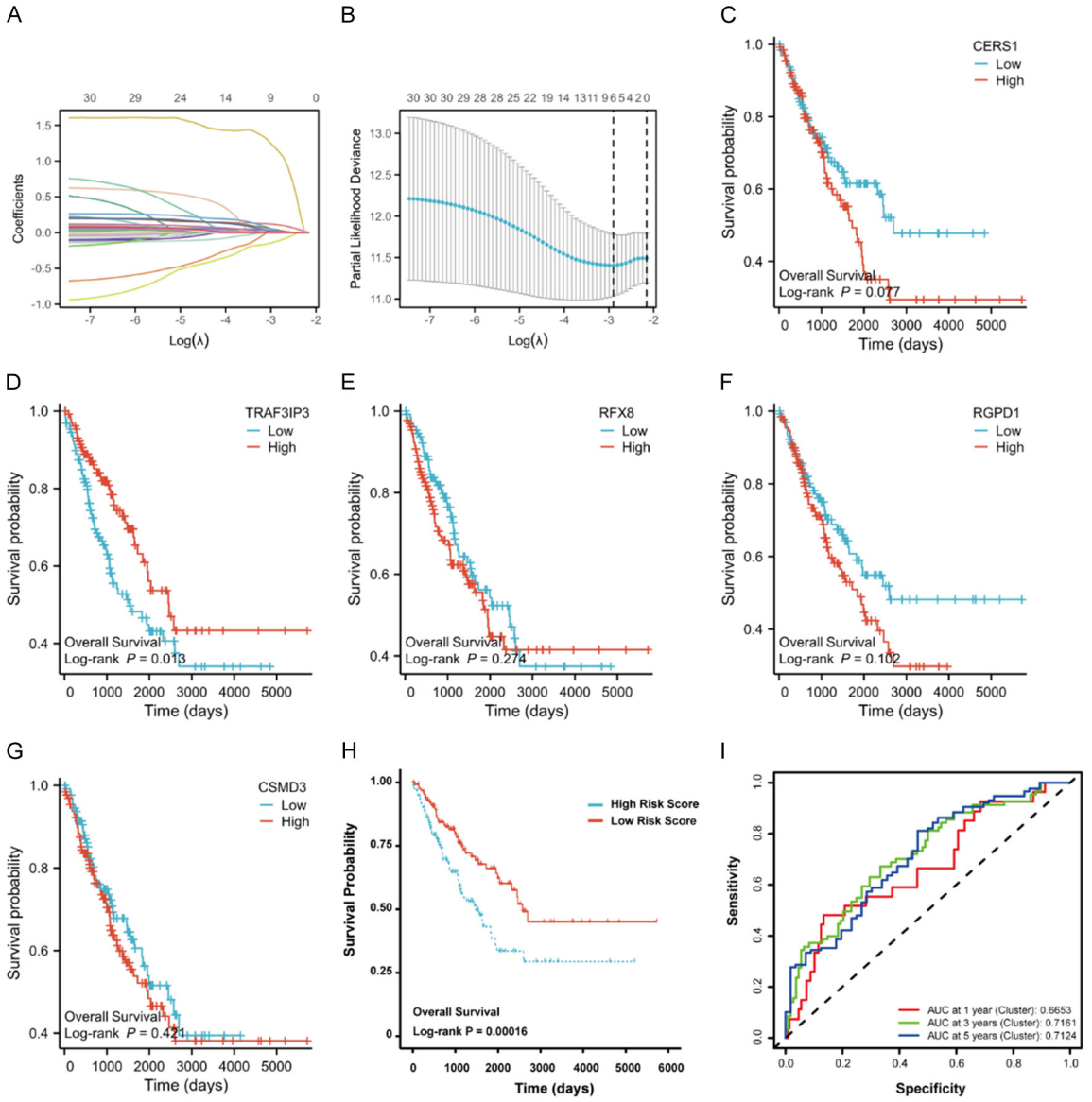

Figure 3. SLC7A5-derived genomic model better predicts the sarcoma prognosis. A. Cross-validation for tuning the parameter selection in the LASSO regression. B. Relative importance of selected genes shown during the Lasso analysis. C-G. Kaplan-Meier survival curves show the correlation between overall survival and the expression level of CERS1, TRAF3IP3, RFX8, RGPD1, and CDMD3. H. Kaplan-Meier survival curves show the correlation between overall survival and risk score calculated by LASSO analysis. I. Time-dependent ROC curves and AUC analyses depict the predictive efficiency of the risk score in TCGA-SARC cohorts. ROC, receiver operating characteristic; AUC, area under the curve; SLC7A5, solute carrier family 7 member 5; TCGA, The Cancer Genome Atlas; SARC, sarcoma; LASSO, least absolute shrinkage and selection operator; CERS1, ceramide synthase 1; TRAF3IP3, tumor necrosis factor receptor-associated factor 3-interacting protein 3; RFX6, regulatory factor X6; RGPD1, RANBP2 like and GRIP domain containing 1; CSMD3, CUB and Sushi multiple domains 3.

SLC7A5 modulates proliferation, apoptosis, migration and invasion in OS cells

We compared SLC7A5 expression in osteosarcoma (OS) cell lines MG63, HOS, and U2OS with that in normal osteoblasts. SLC7A5 was significantly upregulated in all OS cell lines compared with osteoblasts (**Figure 5A**). Following lentiviral transduction, SLC7A5 expression was markedly higher than in untreated cells and the empty vector control group, with consistent results at both the mRNA and protein levels (**Figure 5B**, **5C** and Figure S2A, S2B). CCK-8 assays showed that SLC7A5 overexpression significantly promoted proliferation of MG63 and HOS cells, whereas SLC7A5

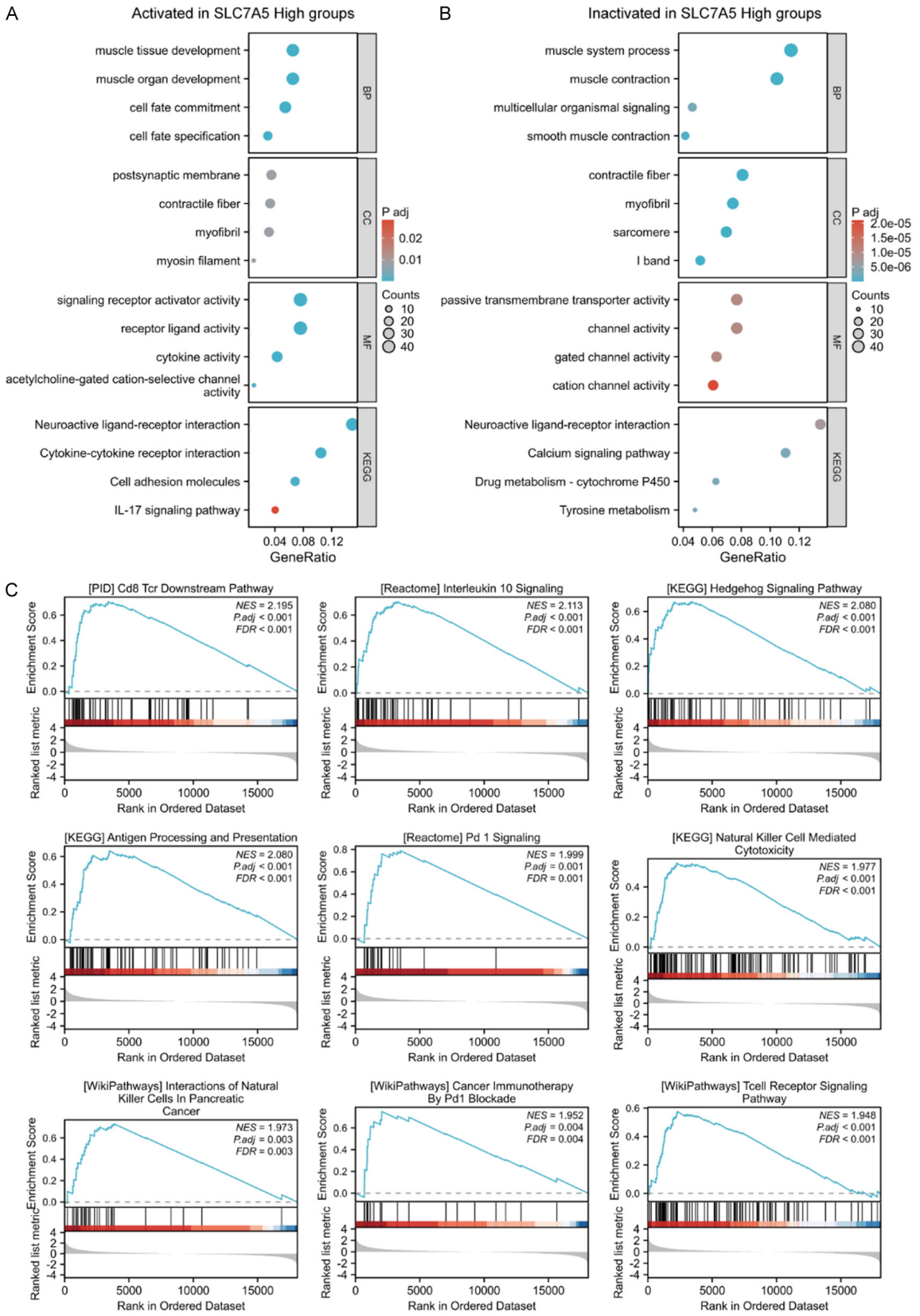

Figure 4. GO, KEGG, and GSEA analyses for DEGs associated with SLC7A5 expression. A. Activated pathways enriched by GO and KEGG using upregulated DEGs in SLC7A5-high TCGA-SARC samples. B. Inactivated pathways enriched by GO and KEGG using downregulated DEGs in SLC7A5-high TCGA-SARC samples. C. Immune-related

pathways associated with SLC7A5 expression selected by GSEA. GO, Gene Ontology; KEGG, Kyoto Encyclopedia of Genes and Genomes; DEGs, differentially expressed genes; GSEA, Gene Set Enrichment Analysis; SLC7A5, solute carrier family 7 member 5; TCGA, The Cancer Genome Atlas; SARC, sarcoma.

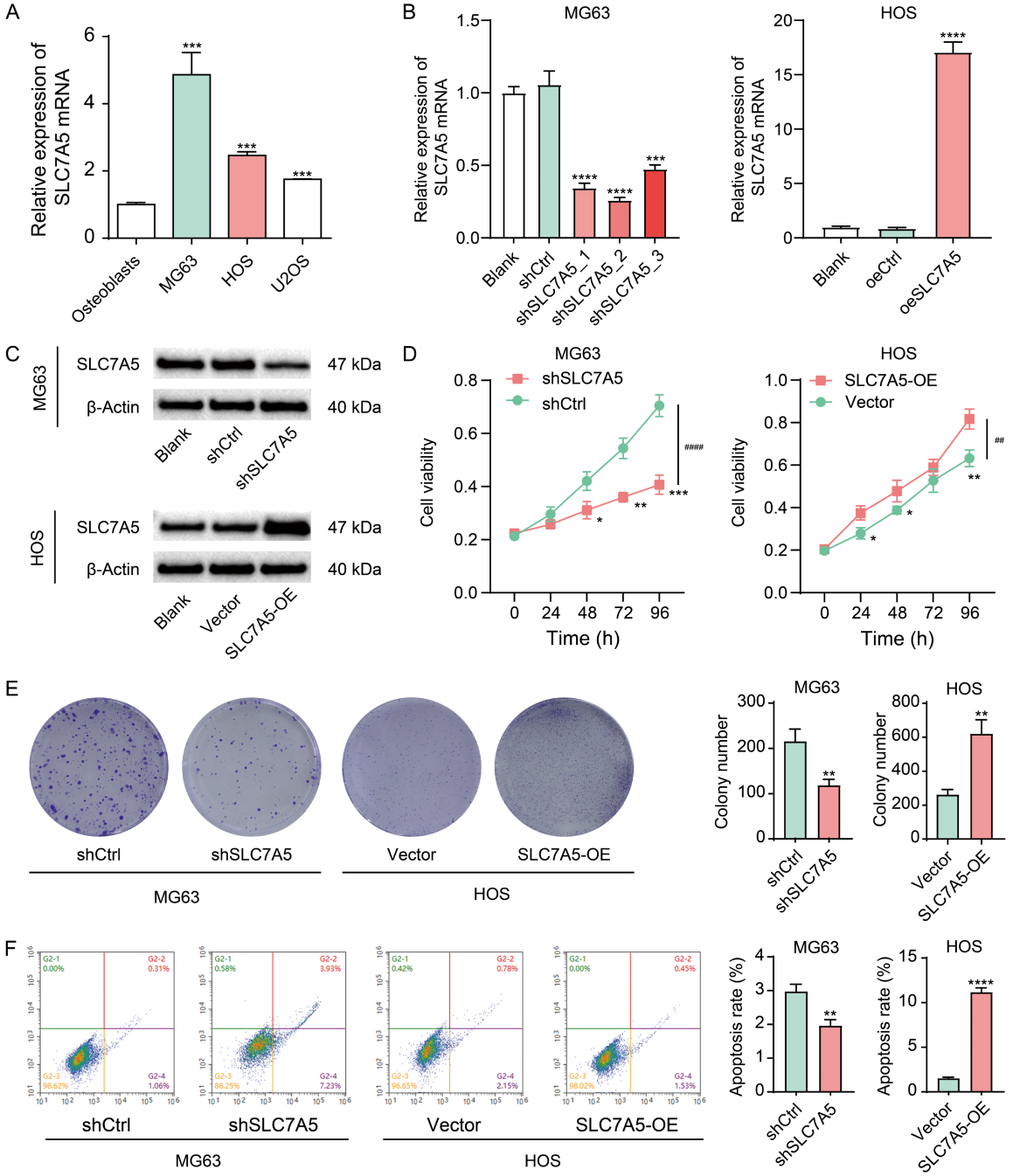

Figure 5. SLC7A5 influences the proliferation and apoptosis of OS cells. A. RT-qPCR analysis of SLC7A5 mRNA expression in OS cell lines versus osteoblasts. B. RT-qPCR detection of SLC7A5 mRNA expression in MG63 and HOS cells following lentivirus-mediated modulation. C. Western blotting of SLC7A5 protein levels in MG63 and HOS cells. D. Cell viability assessed by CCK-8 assay in OS cells with modulated SLC7A5 expression. E. Colony-formation assay of OS cells with differential SLC7A5 expression. F. Apoptosis assay of OS cells with differential SLC7A5 expression. Data are presented as mean ± SD from three independent experiments (n = 3). *P < 0.05, **P < 0.01, ***P < 0.001, ****P < 0.0001 analyzed with Students' t-test. ##P < 0.01, ####P < 0.0001 analyzed with repeated measures ANOVA.

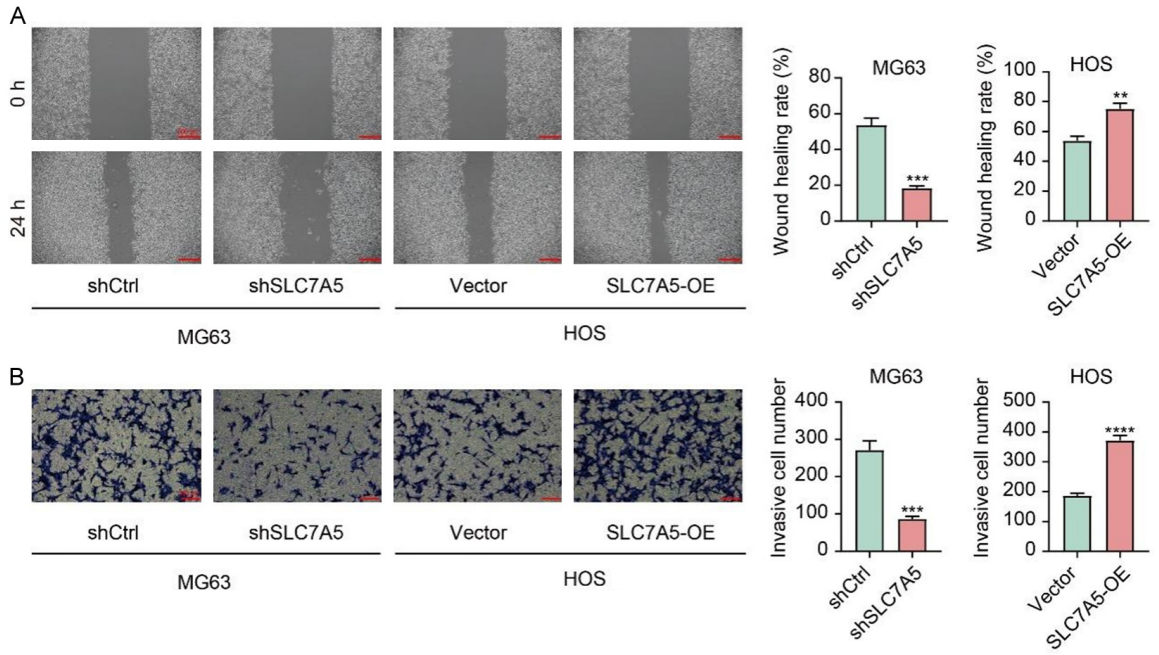

Figure 6. SLC7A5 regulates the migratory and invasive capacities of OS cells. A. Wound healing assay of OS cells with differential SLC7A5 expression. The wound closure area was quantified 24 h after scratching (scale bar = 500 μm). B. Transwell invasion assay of OS cells with differential SLC7A5 expression (scale bar = 100 μm). The number of invasive cells was quantified 24 h after seeding. Data are presented as mean ± SD from three independent experiments (n = 3). **P < 0.01, ***P < 0.001, ****P < 0.0001.

silencing markedly inhibited cell proliferation (**Figure 5D** and Figure S2C). Colony formation assay results were consistent with the CCK-8 findings (**Figure 5E**). Apoptosis was assessed by flow cytometry, revealing a significant increase in apoptosis in MG63 cells, while no obvious change was observed in HOS cells (**Figure 5F**). Further evaluation of cell migration and invasion yielded results consistent with the colony formation assays (**Figure 6**). These findings suggest that SLC7A5 may serve as a potential therapeutic target for inhibiting osteosarcoma metastasis (Figure S3).

SLC7A5 activates mTOR phosphorylation signaling

To investigate the molecular mechanism by which SLC7A5 regulates osteosarcoma progression, transcriptome sequencing was performed on SLC7A5-knockdown MG63 cells and SLC7A5-overexpressing HOS cells. Differentially expressed genes were identified using the criteria of |fold change| > 2 and P < 0.05, and visualized using volcano plots (**Figure 7A**, **7B**). KEGG pathway enrichment analysis revealed that upon SLC7A5 knockdown, We analyzed the enrichment of differentially expressed genes and found that following SLC7A5 knockdown, the affected pathways mainly involved “nucleotide sugar biosynthesis”, “amino sugar and nucleotide sugar metabolism”, and the “mTOR signaling pathway”. Interestingly, after SLC7A5 overexpression, the enriched pathways shifted to “oxidative phosphorylation” and “glycosaminoglycan degradation”, with the mTOR signaling pathway appearing again (**Figure 7C** and **7D**). Given that the mTOR pathway was significantly enriched in both conditions, we further verified its activity via Western blot. The results showed that SLC7A5 knockdown suppressed the phosphorylation levels of mTOR and its downstream effector S6, with little effect on total protein expression. Conversely, SLC7A5 overexpression markedly enhanced the phosphorylation of mTOR and S6 (**Figure 7E** and **7F**).

SLC7A5 promotes in vivo progression of osteosarcoma

We selected 4-week-old BALB/c nude mice and established a tumor model by subcutaneous injection in the right axilla. After the mice had acclimated to the experimental environment for one week, Each mouse was inoculated with

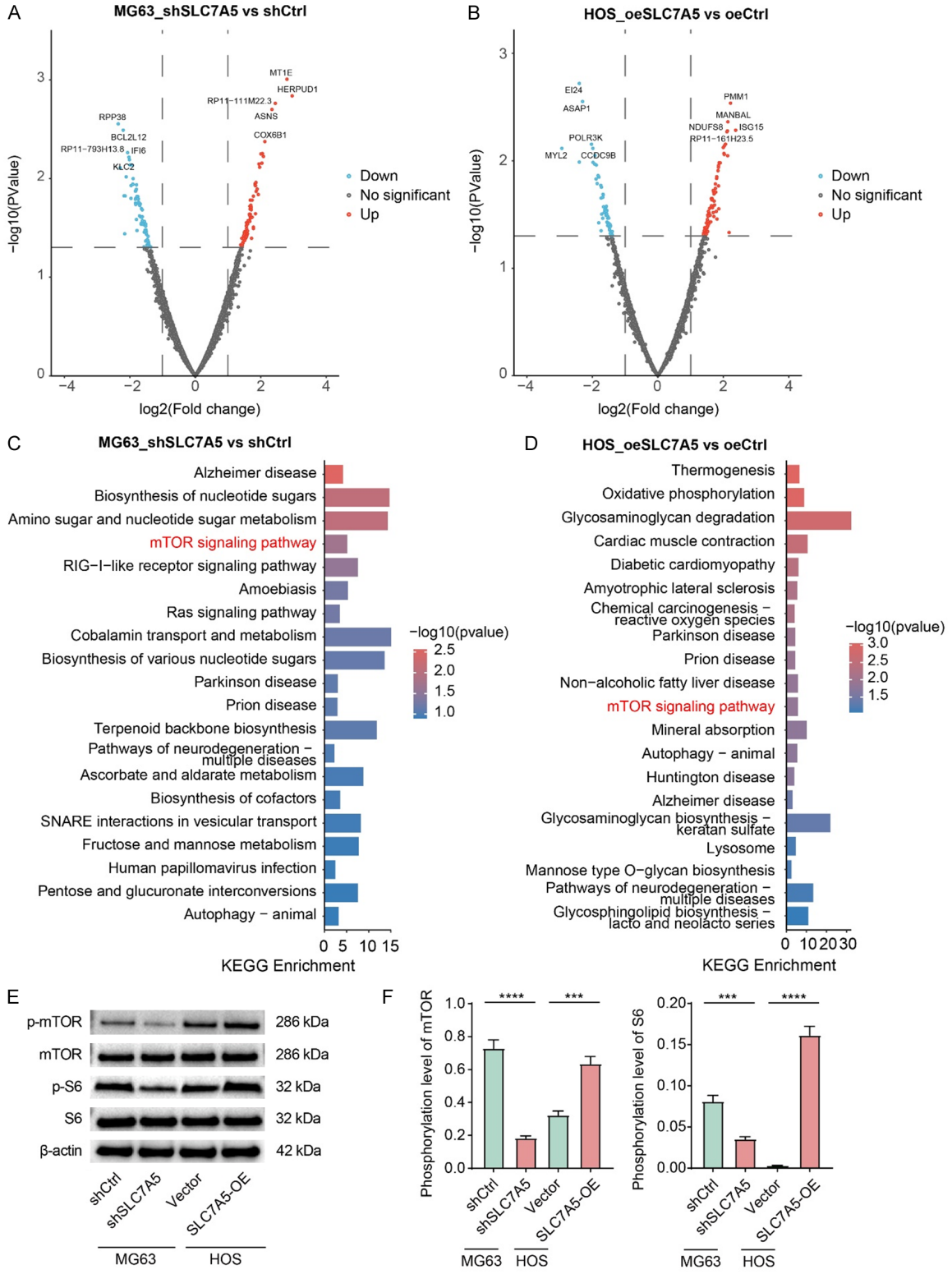

Figure 7. RNA-seq analysis of SLC7A5-mediated transcriptional changes in OS cells. A. Volcano plot of DEGs in MG63 cells after SLC7A5 knockdown. Upregulated genes are shown in red and downregulated genes in blue. B. Volcano plot of DEGs in HOS cells following SLC7A5 overexpression. C. KEGG pathway enrichment analysis of DEGs after SLC7A5 knockdown in MG63 cells. D. KEGG pathway enrichment analysis of DEGs after SLC7A5 knockdown in HOS cells. E. Western blot analysis of the mTOR signaling pathway in OS cells with altered SLC7A5 expression. F. Quantification of phosphorylated mTOR and S6 levels under different SLC7A5 expression conditions. Data are expressed as mean ± SD from three independent experiments (n = 3). ***P < 0.001, ****P < 0.0001.

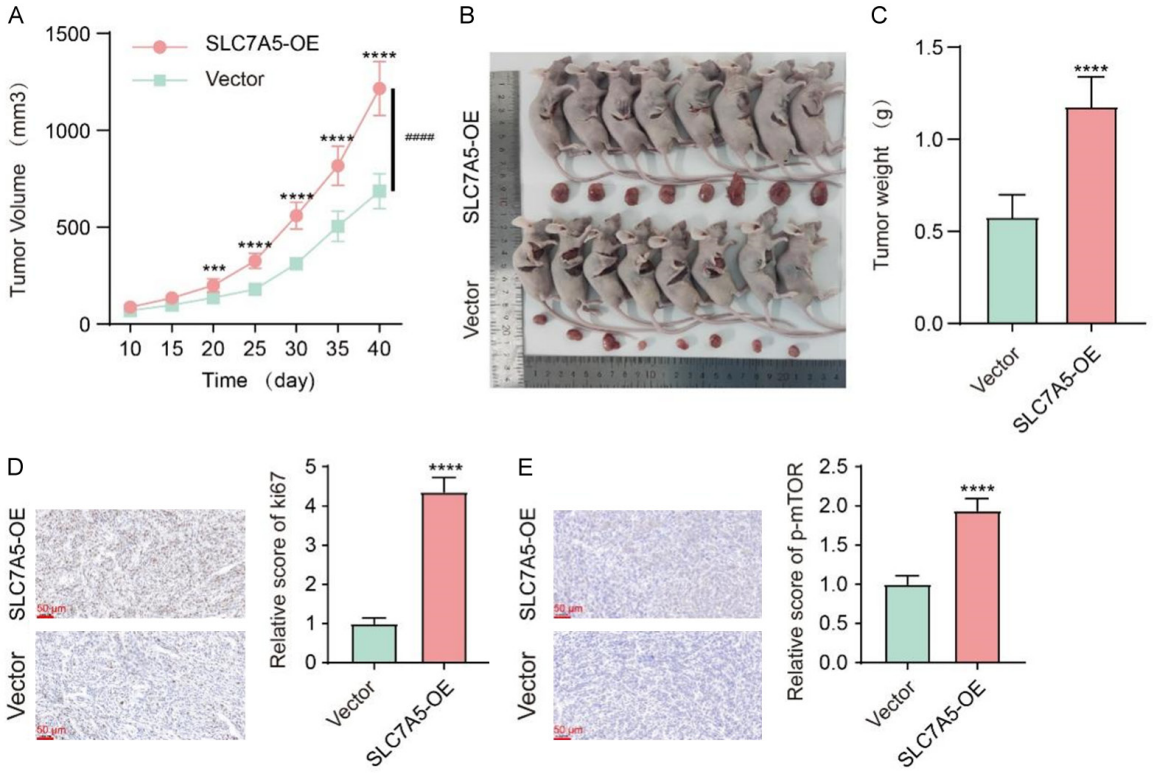

Figure 8. In vivo overexpression of SLC7A5 accelerates tumor progression in a mouse model. A. Tumor volume was measured over time after injecting 2 × 10^6 MG63 cells stably transfected with either empty vector (Vector) or SLC7A5-overexpression vector into BALB/c nude mice. B. Representative bright-field image of tumors excised at day 40 post-injection. C. Final tumor weight at endpoint, showing a significant increase in the SLC7A5-overexpression group compared with the vector control group. D. IHC confirming elevated ki67 protein expression in the overexpression group (scale bar = 50 μm). E. IHC analysis revealing increased p-mTOR expression in the overexpression group (scale bar = 50 μm). Data are presented as mean ± SD (n = 8 mice per group). ***P < 0.001, ****P < 0.0001 analyzed with Students' t-test. ####P < 0.0001 analyzed with repeated measures ANOVA. IHC, immunohistochemistry.

2 × 10^6 cells. Tumor volume was measured every 5 days. On day 40, the mice were euthanized, and the tumors were collected, cleaned, and photographed. The results showed that tumors in the SLC7A5 overexpression group were significantly larger in volume and size and heavier in weight compared with the vector control group (**Figure 8A-C**). Immunohistochemical staining showed that the number of Ki-67-positive cells increased in the SLC7A5 overexpression group, indicating enhanced cell proliferative activity (**Figure 8D**). Phosphorylated mTOR (p-mTOR) was also significantly upregulated, consistent with the RNA-seq and molecular experimental results (**Figure 8E**).

Discussion

By integrating bioinformatics analyses, in vitro experiments, and in vivo animal studies, we systematically investigated the expression patterns, biological functions, and potential therapeutic value of SLC7A5 in osteosarcoma (OS). Analysis of the TCGA database showed that SLC7A5 is significantly upregulated in multiple tumor types; in osteosarcoma, its expression positively correlates with tumor multifocality, distant metastasis, and poor prognosis. A risk score model based on SLC7A5 expression effectively predicted patient survival outcomes. In vitro experiments, including RT-qPCR and Western blotting, confirmed that SLC7A5 expression is markedly higher in MG63, HOS, and U2OS cell lines compared with normal osteoblasts. Functional assays demonstrated that silencing SLC7A5 in MG63 cells significantly inhibited proliferation, colony formation, migration, and invasion, whereas SLC7A5 overexpression produced the opposite effects. In vivo experiments further validated these findings, showing that tumors formed by MG63 cells overexpressing SLC7A5 exhibited signifi-

cantly increased volume and weight. Collectively, these results indicate that SLC7A5 plays a critical role in osteosarcoma progression and may serve as a novel therapeutic target.

SLC7A5 is a critical amino acid transporter that plays an important regulatory role in cellular metabolism and various biological processes [35]. It is primarily localized to the plasma membrane of cancer cells and is upregulated in multiple malignancies, including breast cancer, head and neck squamous cell carcinoma, and bladder cancer [36-39]. Studies have shown that SLC7A5 is an essential factor for the growth of KRAS-mutant colorectal cancer [40]. Ma and Wu et al. demonstrated that in gastric cancer, SLC7A5 promotes tumor proliferation through interaction with IGF2BP3 [23, 41]. Gai et al. indicated that SLC7A5 influences therapeutic responses in non-small cell lung cancer by regulating amino acid metabolism [42]. In tumors such as breast cancer and bladder cancer, SLC7A5 expression is closely associated with immune evasion mechanisms and immunotherapy response, affecting the efficacy of anti-PD-1 immunotherapy by modulating the tumor immune microenvironment [36, 43, 44]. Jiang and Huang et al. demonstrated that in triple-negative breast cancer, SLC7A5 improves the sensitivity of the tumor to treatment by promoting cross-regulation of amino acid metabolism [43, 44]. SLC7A5 plays a role in tumor treatment resistance. Zhou et al. confirmed that in certain cancers, SLC7A5, in conjunction with other molecules, enhances the resistance of the tumor to chemotherapy and radiotherapy [45]. At the functional mechanism level, SLC7A5 mediates the uptake of essential amino acids such as leucine and phenylalanine, and is closely associated with the mTORC1 signaling pathway, thereby regulating protein synthesis and cell growth [40, 46, 47]. In the present study, RNA-seq analysis of MG63 cells following SLC7A5 knockdown and HOS cells after SLC7A5 overexpression revealed significant enrichment of the mTOR signaling pathway in KEGG analysis of differentially expressed genes. Subsequent western blot experiments demonstrated that SLC7A5 OE promotes phosphorylation of mTOR and its downstream target S6, whereas SLC7A5 knockdown suppresses mTOR phosphorylation.

The cancer-specific expression of SLC7A5 provides an important basis for its application in clinical diagnosis. Jin et al. have shown that PET imaging using SLC7A5-specific tracers, such as FAMT, can effectively distinguish malignant tumors from benign inflammatory lesions [48], highlighting its significant potential in precision tumor imaging. In terms of therapy, targeting SLC7A5 shows promising prospects. Preclinical studies have mainly focused on small-molecule inhibitors and SLC7A5-conjugated antitumor drugs. Zhang and Saito et al reported that the SLC7A5-specific inhibitor JPH095 demonstrated significant antitumor activity with minimal toxicity in in vivo experiments [49, 50], suggesting it could serve as a potential new strategy for treatment-resistant tumors. Structural studies of SLC7A5, particularly cryo-electron microscopy (cryo-EM) analyses, provide a solid foundation for designing more selective and effective inhibitors [51]. SLC7A5 has also been shown to mediate targeted delivery of antitumor drugs-for example, facilitating the uptake of L-4-boronophenylalanine in boron neutron capture therapy [27]. further expanding its potential applications in precision therapy. Taken together, SLC7A5 represents a highly promising target for both diagnosis and treatment, especially in malignancies that rely on its activity for growth. Treatment of osteosarcoma is gradually advancing into molecular targeted therapy and immunotherapy. Medical progress is increasing the clinical feasibility of personalized treatment strategies. As an important therapeutic target, SLC7A5 can potentially be combined with immune checkpoint inhibitors or CAR-T therapy. Further exploration of its regulatory role in the osteosarcoma immune microenvironment may enhance antitumor immune responses. In addition, incorporating SLC7A5 into prognostic models could improve early diagnosis and enhance the precision of individualized therapy.

Although multiple biomarkers, such as RAMP1 [52], SMARCB1 [53], have been proposed to predict therapeutic responses in osteosarcoma, their clinical application remains limited. Our study indicates that SLC7A5 plays a central role in the occurrence and progression of osteosarcoma. High SLC7A5 expression not only affects tumor behavior and patient prognosis but also regulates the immune microenvironment. Prognostic models based on SLC7A5 show significantly improved predictive accuracy, offering new directions for optimizing osteo-

sarcoma treatment strategies and improving patient outcomes.

However, several limitations remain. The prognostic model was developed solely using the TCGA-SARC retrospective dataset, lacking external validation in an osteosarcoma-specific cohort. Analyses were primarily conducted at the mRNA level, without including protein expression or multicenter clinical samples. While in vitro experiments demonstrated that SLC7A5 overexpression promotes tumor proliferation and immune evasion, the underlying regulatory mechanisms still require verification in vivo. The causal relationship between SLC7A5 expression and immune cell infiltration remains unclear, and inconsistencies regarding the roles of TFH cells and CD56-dim NK cells suggest that the associated immune regulatory network needs further investigation.

Acknowledgements

We thank the financial support from Nantong University.

The study was supported by grants from the Nantong First People's Hospital Provincial and Ministerial Level High-level Science and Technology Project Cultivation Fund granted for Ziliang Yu (YPYJJYB23002), the Nantong University Special Research Fund for Clinical Medicine (Grant No. 2024JY003), the Research Project of Nantong Municipal Health Commission for Haiping Zhang (MB2021023), and the Nantong Youth Medical Expert Project granted for Haiping Zhang.

Disclosure of conflict of interest

None.

Abbreviations

ANOVA, Analysis of Variance; BCA, Bicinchoninic acid; BPs, biological processes; CCs, cellular components; Cox, Cox proportional hazards model; DESeq2, Differential Expression Analysis for Sequence Count Data; FDR, False discovery rate; GO, Gene Ontology; KEGG, Kyoto Encyclopedia of Genes and Genomes; LAT1, Large neutral amino acid transporter 1; LASSO, Least Absolute Shrinkage and Selection Operator; Log-rank, Log-rank test; MFs, molecular functions; mRNA, Messenger RNA; NES, Normalized enrichment score; NK, natural killer; OS, osteosarcoma; PET, Positron emission tomography; PVDF, Polyvinylidene fluoride; RIPA, Radioimmunoprecipitation assay; ROC, Receiver operating characteristic; SLC7A5, Solute carrier family 7 member 5; ssGSEA, Single-sample Gene Set Enrichment Analysis; TCGA, The Cancer Genome Atlas; TIL, Tumor-Infiltrating Lymphocyte; TPM, Transcripts per million; Treg, Regulatory T cells.

Address correspondence to: Haiping Zhang, Department of Orthopedic Surgery, Nantong First People's Hospital, Affiliated Hospital 2 of Nantong University, No. 666 Shengli Road, Nantong 226000, Jiangsu, China. E-mail: zhanghaipingx@163.com

References

[1] Xu Y, Shi F, Zhang Y, Yin M, Han X, Feng J and Wang G. Twenty-year outcome of prevalence, incidence, mortality and survival rate in patients with malignant bone tumors. Int J Cancer 2024; 154: 226-240.

[2] Sheng G, Gao Y, Yang Y and Wu H. Osteosarcoma and metastasis. Front Oncol 2021; 11: 780264.

[3] Wang T, Huang J, Chen G, Fu J, Li T, Zou X and Yi H. miR-1293 suppresses osteosarcoma progression by modulating drug sensitivity in response to cisplatin treatment. Int Immunopharmacol 2024; 130: 111702.

[4] Klangjorhor J, Pongnikorn D, Phanphaisarn A, Chaiyawat P, Teeyakasem P, Suksakit P, Pasena A, Udomruk S, Orrapin S, Pornwattanavate S, Waisri N, Daoprasert K, Wisanuyotin T, Santong C, Sangrajrang S, Sitthikong S, Tuntarattanapong P, Prechawittayakul P and Pruksakorn D. An analysis of the incidence and survival rates of bone sarcoma patients in thailand: reports from population-based cancer registries 2001-2015. Cancer Epidemiol 2022; 76: 102056.

[5] Kollar A, Rothermundt C, Klenke F, Bode B, Baumhoer D, Arndt V, Feller A and Group NW. Incidence, mortality, and survival trends of soft tissue and bone sarcoma in Switzerland between 1996 and 2015. Cancer Epidemiol 2019; 63: 101596.

[6] Bian J, Liu Y, Zhao X, Meng C, Zhang Y, Duan Y and Wang G. Research progress in the mechanism and treatment of osteosarcoma. Chin Med J (Engl) 2023; 136: 2412-2420.

[7] Jin J, Cong J, Lei S, Zhang Q, Zhong X, Su Y, Lu M, Ma Y, Li Z, Wang L, Zhu N and Yang J. Cracking the code: deciphering the role of the tumor microenvironment in osteosarcoma metasta-

sis. Int Immunopharmacol 2023; 121: 110422.
[8] Zeng J, Peng Y, Wang D, Ayesha K and Chen S. The interaction between osteosarcoma and other cells in the bone microenvironment: from mechanism to clinical applications. Front Cell Dev Biol 2023; 11: 1123065.
[9] Park JA and Cheung NV. Promise and challenges of T cell immunotherapy for osteosarcoma. Int J Mol Sci 2023; 24: 12520.
[10] Zhu J, Fan J, Xia Y, Wang H, Li Y, Feng Z and Fu C. Potential targets and applications of nanodrug targeting myeloid cells in osteosarcoma for the enhancement of immunotherapy. Front Pharmacol 2023; 14: 1271321.
[11] Anand N, Peh KH and Kolesar JM. Macrophage repolarization as a therapeutic strategy for osteosarcoma. Int J Mol Sci 2023; 24: 2858.
[12] Irac SE, Oksa A, Jackson K, Herndon A, Allavena R and Palmieri C. Cytokine expression in canine lymphoma, osteosarcoma, mammary gland tumour and melanoma: comparative aspects. Vet Sci 2019; 6: 37.
[13] Gao X, Gao B and Li S. Extracellular vesicles: a new diagnostic biomarker and targeted drug in osteosarcoma. Front Immunol 2022; 13: 1002742.
[14] Astolfi A, Nannini M, Indio V, Schipani A, Rizzo A, Perrone AM, De Iaco P, Pirini MG, De Leo A, Urbini M, Secchiero P and Pantaleo MA. Genomic database analysis of uterine leiomyosarcoma mutational profile. Cancers (Basel) 2020; 12: 2126.
[15] Rizzo A, Nannini M, Astolfi A, Indio V, De Iaco P, Perrone AM, De Leo A, Incorvaia L, Di Scioscio V and Pantaleo MA. Impact of chemotherapy in the adjuvant setting of early stage uterine leiomyosarcoma: a systematic review and updated meta-analysis. Cancers (Basel) 2020; 12: 1899.
[16] Bas O, Sahin TK, Karahan L, Rizzo A and Guven DC. Prognostic significance of the cachexia index (CXI) in patients with cancer: a systematic review and meta-analysis. Clin Nutr ESPEN 2025; 68: 240-247.
[17] Sahin TK, Rizzo A, Aksoy S and Guven DC. Prognostic significance of the royal marsden hospital (RMH) score in patients with cancer: a systematic review and meta-analysis. Cancers (Basel) 2024; 16: 1835.
[18] Sahin TK, Ayasun R, Rizzo A and Guven DC. Prognostic value of neutrophil-to-eosinophil ratio (NER) in cancer: a systematic review and meta-analysis. Cancers (Basel) 2024; 16: 3689.
[19] Napolitano L, Galluccio M, Scalise M, Parravicini C, Palazzolo L, Eberini I and Indiveri C. Novel insights into the transport mechanism of the human amino acid transporter LAT1 (SLC7A5). Probing critical residues for substrate translocation. Biochim Biophys Acta Gen Subj 2017; 1861: 727-736.
[20] Scanga R, Scalise M, Marino N, Parisi F, Barca D, Galluccio M, Brunocilla C, Console L and Indiveri C. LAT1 (SLC7A5) catalyzes copper (histidinate) transport switching from antiport to uniport mechanism. iScience 2023; 26: 107738.
[21] Dickens D, Webb SD, Antonyuk S, Giannoudis A, Owen A, Radisch S, Hasnain SS and Pirmohamed M. Transport of gabapentin by LAT1 (SLC7A5). Biochem Pharmacol 2013; 85: 1672-1683.
[22] Liu D, Ren H, Wen G and Xia P. Nicotine upregulates SLC7A5 expression depending on TRIM29 in non-small cell lung cancer. Genes Dis 2024; 11: 582-584.
[23] Ma Q, Yang F, Huang B, Pan X, Li W, Yu T, Wang X, Ran L, Qian K, Li H, Li H, Liu Y, Liang C, Ren J, Zhang Y, Wang S and Xiao B. CircARID1A binds to IGF2BP3 in gastric cancer and promotes cancer proliferation by forming a circARID1A-IGF2BP3-SLC7A5 RNA-protein ternary complex. J Exp Clin Cancer Res 2022; 41: 251.
[24] Liang M, Wang H, Liu C, Lei T and Min J. OIP5-AS1 contributes to the development in endometrial carcinoma cells by targeting miR-152-3p to up-regulate SLC7A5. Cancer Cell Int 2021; 21: 440.
[25] Li C, Chen S, Jia W, Li W, Wei D, Cao S, Qian Y, Guan R, Liu H and Lei D. Identify metabolism-related genes IDO1, ALDH2, NCOA2, SLC7A5, SLC3A2, LDHB, and HPRT1 as potential prognostic markers and correlate with immune infiltrates in head and neck squamous cell carcinoma. Front Immunol 2022; 13: 955614.
[26] Zhu Q, Wang J, Shi Y, Zha X and Wang S. Bioinformatics prediction and in vivo verification identify SLC7A5 as immune infiltration related biomarker in breast cancer. Cancer Manag Res 2022; 14: 2545-2559.
[27] Kanai Y. Amino acid transporter LAT1 (SLC7A5) as a molecular target for cancer diagnosis and therapeutics. Pharmacol Ther 2022; 230: 107964.
[28] Zhang W, Cao X, Zhong X, Wu H, Shi Y, Feng M, Wang YC, Ann D, Gwack Y, Yuan YC, Shang W and Sun Z. SRC2 controls CD4(+) T cell activation via stimulating c-Myc-mediated upregulation of amino acid transporter Slc7a5. Proc Natl Acad Sci U S A 2023; 120: e2221352120.
[29] Broer A, Rahimi F and Broer S. Deletion of amino acid transporter ASCT2 (SLC1A5) reveals an essential role for transporters SNAT1 (SLC38A1) and SNAT2 (SLC38A2) to sustain glutaminolysis in cancer cells. J Biol Chem 2016; 291: 13194-13205.

[30] Endo-Munoz L, Cumming A, Sommerville S, Dickinson I and Saunders NA. Osteosarcoma is characterised by reduced expression of markers of osteoclastogenesis and antigen presentation compared with normal bone. Br J Cancer 2010; 103: 73-81.
[31] Scott MC, Temiz NA, Sarver AE, LaRue RS, Rathe SK, Varshney J, Wolf NK, Moriarity BS, O'Brien TD, Spector LG, Largaespada DA, Modiano JF, Subramanian S and Sarver AL. Comparative transcriptome analysis quantifies immune cell transcript levels, metastatic progression, and survival in osteosarcoma. Cancer Res 2018; 78: 326-337.
[32] Ho XD, Phung P, Q Le V, H Nguyen V, Reimann E, Prans E, Kõks G, Maasalu K, Le NT, H Trinh L, G Nguyen H, Märtson A and Kõks S. Whole transcriptome analysis identifies differentially regulated networks between osteosarcoma and normal bone samples. Exp Biol Med (Maywood) 2017; 242: 1802-1811.
[33] Gholami A, Mohkam M, Soleimanian S, Sadraeian M and Lauto A. Bacterial nanotechnology as a paradigm in targeted cancer therapeutic delivery and immunotherapy. Microsyst Nanoeng 2024; 10: 113.
[34] Liang H, Cui M, Tu J and Chen X. Advancements in osteosarcoma management: integrating immune microenvironment insights with immunotherapeutic strategies. Front Cell Dev Biol 2024; 12: 1394339.
[35] Cappoli N, Jenkinson MD, Dello Russo C and Dickens D. LAT1, a novel pharmacological target for the treatment of glioblastoma. Biochem Pharmacol 2022; 201: 115103.
[36] Zhang C, Wang Y, Guo X, Wang Z, Xiao J and Liu Z. SLC7A5 correlated with malignancies and immunotherapy response in bladder cancer. Cancer Cell Int 2024; 24: 182.
[37] Wu Q, Luo Y, Lin N, Zheng S and Xie X. Prognostic value and immune signatures of anoikis-related genes in breast cancer. J Immunother 2024; 47: 328-341.
[38] Nam C, Li LY, Yang Q, Ziman B, Zhao H, Hu B, Collet C, Jing P, Lei Q, Xu LY, Li EM, Koeffler HP, Sinha UK and Lin DC. A druggable cascade links methionine metabolism to epigenomic reprogramming in squamous cell carcinoma. Proc Natl Acad Sci U S A 2024; 121: e2320835121.
[39] El Ansari R, Craze ML, Miligy I, Diez-Rodriguez M, Nolan CC, Ellis IO, Rakha EA and Green AR. The amino acid transporter SLC7A5 confers a poor prognosis in the highly proliferative breast cancer subtypes and is a key therapeutic target in luminal B tumours. Breast Cancer Res 2018; 20: 21.
[40] Najumudeen AK, Ceteci F, Fey SK, Hamm G, Steven RT, Hall H, Nikula CJ, Dexter A, Murta T, Race AM, Sumpton D, Vlahov N, Gay DM, Knight JRP, Jackstadt R, Leach JDG, Ridgway RA, Johnson ER, Nixon C, Hedley A, Gilroy K, Clark W, Malla SB, Dunne PD, Rodriguez-Blanco G, Critchlow SE, Mrowinska A, Malviya G, Solovyev D, Brown G, Lewis DY, Mackay GM, Strathdee D, Tardito S, Gottlieb E; CRUK Rosetta Grand Challenge Consortium; Takats Z, Barry ST, Goodwin RJA, Bunch J, Bushell M, Campbell AD and Sansom OJ. The amino acid transporter SLC7A5 is required for efficient growth of KRAS-mutant colorectal cancer. Nat Genet 2021; 53: 16-26.
[41] Wu X, Fang Y, Gu Y, Shen H, Xu Y, Xu T, Shi R, Xu D, Zhang J, Leng K, Shu Y and Ma P. Fat mass and obesity-associated protein (FTO) mediated m(6)A modification of circFAM192A promoted gastric cancer proliferation by suppressing SLC7A5 decay. Mol Biomed 2024; 5: 11.
[42] Gai X, Liu Y, Lan X, Chen L, Yuan T, Xu J, Li Y, Zheng Y, Yan Y, Yang L, Fu Y, Tang S, Cao S, Dai X, Zhu H, Geng M, Ding J, Pu C and Huang M. Oncogenic KRAS induces arginine auxotrophy and confers a therapeutic vulnerability to SLC7A1 inhibition in non-small cell lung cancer. Cancer Res 2024; 84: 1963-1977.
[43] Jiang C, Qian Y, Bai X, Li S, Zhang L, Xie Y, Lu Y, Lu Z, Liu B and Jiang BH. SLC7A5/E2F1/PTBP1/PKM2 axis mediates progression and therapy effect of triple-negative breast cancer through the crosstalk of amino acid metabolism and glycolysis pathway. Cancer Lett 2025; 617: 217612.
[44] Huang R, Wang H, Hong J, Wu J, Huang O, He J, Chen W, Li Y, Chen X, Shen K and Wang Z. Targeting glutamine metabolic reprogramming of SLC7A5 enhances the efficacy of anti-PD-1 in triple-negative breast cancer. Front Immunol 2023; 14: 1251643.
[45] Zhou Z, Zhang B, Deng Y, Deng S, Li J, Wei W, Wang Y, Wang J, Feng Z, Che M, Yang X, Meng J, Li Y, Hu Y, Sun Y, Wen L, Huang F, Sheng Y, Wan C and Yang K. FBW7/GSK3β mediated degradation of IGF2BP2 inhibits IGF2BP2-SLC7A5 positive feedback loop and radioresistance in lung cancer. J Exp Clin Cancer Res 2024; 43: 34.
[46] Jin J, Kim C, Xia Q, Gould TM, Cao W, Zhang H, Li X, Weiskopf D, Grifoni A, Sette A, Weyand CM and Goronzy JJ. Activation of mTORC1 at late endosomes misdirects T cell fate decision in older individuals. Sci Immunol 2021; 6: eabg0791.
[47] Yang B, Wang Z, Niu K, Li T, Tong T, Li S, Su L, Wang Y, Shen C, Jin X, Song J and Lu X. TRIM35 triggers cardiac remodeling by regulating SLC7A5-mediated amino acid transport and mTORC1 activation in fibroblasts. Cell Commun Signal 2024; 22: 444.

[48] Jin C, Wei L, Ohgaki R, Tominaga H, Xu M, Okuda S, Okanishi H, Kawamoto Y, He X, Nagamori S and Kanai Y. Interaction of halogenated tyrosine/phenylalanine derivatives with organic anion transporter 1 in the renal handling of tumor imaging probes. J Pharmacol Exp Ther 2020; 375: 451-462.

[49] Zhang YW, Velasco-Hernandez T, Mess J, Lalioti ME, Romero-Mulero MC, Obier N, Karantzelis N, Rettkowski J, Schönberger K, Karabacz N, Jäcklein K, Morishima T, Trincado JL, Romecin P, Martinez A, Takizawa H, Shoumariyeh K, Renders S, Zeiser R, Pahl HL, Béliveau F, Hébert J, Lehnertz B, Sauvageau G, Menendez P and Cabezas-Wallscheid N. GPRC5C drives branched-chain amino acid metabolism in leukemogenesis. Blood Adv 2023; 7: 7525-7538.

[50] Saito S, Ando K, Sakamoto S, Xu M, Yamada Y, Rii J, Kanaoka S, Wei J, Zhao X, Pae S, Kanesaka M, Goto Y, Sazuka T, Imamura Y, Reien Y, Hamaguchi-Suzuki N, Saito S, Hirayama Y, Hashimoto H, Kanai Y, Ichikawa T and Anzai N. The LAT1 inhibitor JPH203 suppresses the growth of castration-resistant prostate cancer through a CD24-mediated mechanism. Cancer Sci 2024; 115: 2461-2472.

[51] Lee Y, Wiriyasermkul P, Jin C, Quan L, Ohgaki R, Okuda S, Kusakizako T, Nishizawa T, Oda K, Ishitani R, Yokoyama T, Nakane T, Shirouzu M, Endou H, Nagamori S, Kanai Y and Nureki O. Cryo-EM structure of the human L-type amino acid transporter 1 in complex with glycoprotein CD98hc. Nat Struct Mol Biol 2019; 26: 510-517.

[52] Xie L, Xiao W, Fang H and Liu G. RAMP1 as a novel prognostic biomarker in pan-cancer and osteosarcoma. PLoS One 2023; 18: e0292452.

[53] Guo T, Wei R, Dean DC, Hornicek FJ and Duan Z. SMARCB1 expression is a novel diagnostic and prognostic biomarker for osteosarcoma. Biosci Rep 2022; 42: BSR20212446.

Table S1. Top 10 upregulated genes and top 10 downregulated genes in TCGA-SARC tissues with different expression levels of SLC7A5

Gene_name	BaseMean	Log2FoldChange	LfcSE	Stat	*P* value	Padj
ARHGAP36	42.19001	4.258172	0.431364	9.871409	5.54E-23	7.27E-19
PMP2	29.16638	3.765595	0.729973	5.158541	2.49E-07	1.26E-05
CGB8	2.900273	3.679951	0.69368	5.304967	1.13E-07	6.82E-06
SALL3	21.50873	3.54821	0.60538	5.861131	4.6E-09	5.45E-07
CDH19	52.17913	3.410225	0.606813	5.619893	1.91E-08	1.64E-06
LCE2A	2.823296	3.350923	0.916989	3.654268	0.000258	0.002796
BPIFB4	198.6161	3.300207	0.486637	6.781658	1.19E-11	4.81E-09
PSG1	39.24316	3.206243	0.563057	5.694353	1.24E-08	1.18E-06
CHRNA1	320.6263	3.138085	0.347516	9.030055	1.72E-19	9.65E-16
PSG5	64.80861	3.107317	0.574293	5.410686	6.28E-08	4.23E-06
SERTM2	8139.97	-2.74905	0.525507	-5.23123	1.68E-07	9.29E-06
TCF23	1128.518	-2.78103	0.387402	-7.17868	7.04E-13	4.62E-10
FBXO40	22.92943	-2.9365	0.347969	-8.43898	3.2E-17	7.88E-14
ACTA1	3687.331	-2.93964	0.392462	-7.49026	6.87E-14	6.4E-11
BRS3	8.109284	-3.04206	0.437329	-6.95599	3.5E-12	1.79E-09
PAGE4	12.53769	-3.09517	0.673603	-4.59495	4.33E-06	0.000121
ADIPOQ	39.69009	-3.50635	0.590545	-5.93749	2.89E-09	3.79E-07
TAC3	43.43186	-3.8423	0.348061	-11.0391	2.47E-28	4.87E-24
PRLHR	6.028619	-4.17445	0.497442	-8.39184	4.79E-17	1.11E-13
KRT77	4.526355	-4.53522	0.750393	-6.04379	1.51E-09	2.29E-07

Table S2. The top seven positively correlated genes and the top seven negatively correlated genes were screened by Spearman's correlation analysis

Gene_name	Correlation_pearson	*P*value_pearson	Padj_pearson	Correlation_spearman	Palue_spearman	Pdj_spearman
SLC7A5	1	0	0	1	0	0
PSAT1	0.557840899	6.53701E-23	1.86289E-18	0.554501785	0	0
AUNIP	0.511973163	5.64718E-19	6.43722E-15	0.501952017	3.42984E-18	6.30593E-15
TPM3	0.48092194	1.25347E-16	8.9302E-13	0.494459514	0	0
RELT	0.51631807	2.53544E-19	4.81691E-15	0.491401989	0	0
TUBA1C	0.490342974	2.57791E-17	2.09897E-13	0.486562062	0	0
RCC2	0.512266043	5.35235E-19	6.43722E-15	0.48408174	0	0
HMGB3	0.497311795	7.752E-18	7.36376E-14	0.476206716	0	0
PDE1B	-0.406161537	7.22476E-12	4.39516E-09	-0.376262919	3.90824E-10	1.01712E-07
THRB	-0.392389164	4.11844E-11	1.58602E-08	-0.383299578	1.24397E-10	4.00567E-08
CPO	-0.393702577	3.50058E-11	1.44577E-08	-0.394672859	3.10305E-11	1.39259E-08
AOC3	-0.407652469	5.95508E-12	3.77122E-09	-0.395918155	3.76266E-11	1.62464E-08
ACBD4	-0.409399586	4.74239E-12	3.10681E-09	-0.408951721	6.94846E-12	4.44974E-09
NENF	-0.403260207	1.04947E-11	5.80726E-09	-0.415205299	2.90229E-12	2.09388E-09
METTL7A	-0.403634752	1.00029E-11	5.58939E-09	-0.425520406	5.81686E-13	6.25971E-10

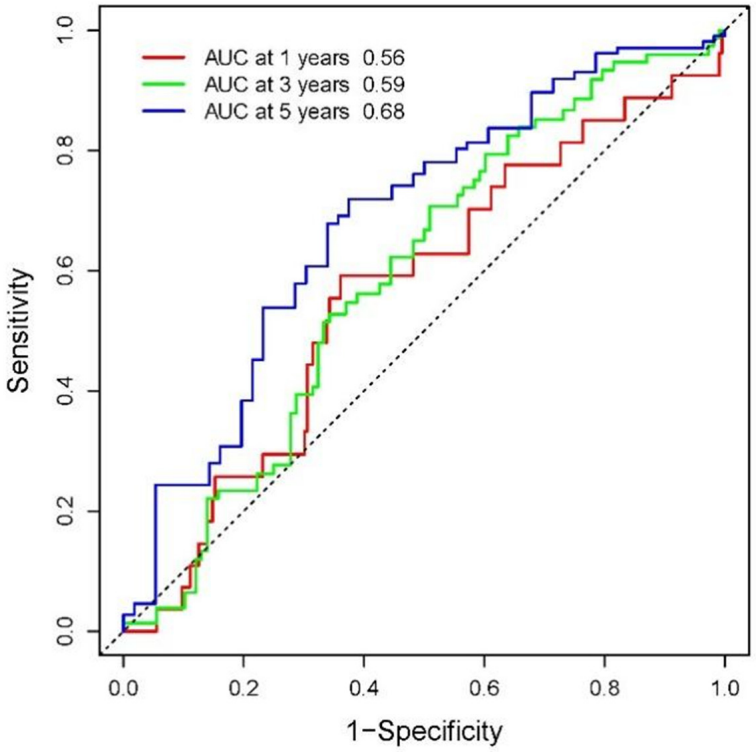

Figure S1. Time-dependent ROC curves and AUC analyses depicting the predictive efficiency of SLC7A5 in TCGA-SARC cohorts. SLC7A5, solute carrier family 7 member 5; TCGA, The Cancer Genome Atlas; SARC, sarcoma; ROC, receiver operating characteristic; AUC, area under the curve.

Table S3. Pathways associated with SLC7A5 expression enriched by GO and KEGG analysis

Status	ONTOLOGY	ID	Description	GeneRatio	*p* value	p.adjust	q value
Activated	BP	GO:0007517	muscle organ development	37/567	9.13E-12	3.69E-08	3.22E-08
Activated	BP	GO:0045165	cell fate commitment	31/567	1.28E-10	2.58E-07	2.25E-07
Activated	BP	GO:0060537	muscle tissue development	37/567	2.25E-09	3.04E-06	2.65E-06
Activated	BP	GO:0001708	cell fate specification	17/567	3.81E-09	3.85E-06	3.36E-06
Activated	CC	GO:0032982	myosin filament	6/600	3.95E-05	0.007863	0.006732
Activated	CC	GO:0043292	contractile fiber	20/600	4.72E-05	0.007863	0.006732
Activated	CC	GO:0030016	myofibril	19/600	8.11E-05	0.007863	0.006732
Activated	CC	GO:0045211	postsynaptic membrane	21/600	9.93E-05	0.007863	0.006732
Activated	MF	GO:0048018	receptor ligand activity	44/579	3.98E-10	1.86E-07	1.66E-07
Activated	MF	GO:0030546	signaling receptor activator activity	44/579	6.23E-10	1.86E-07	1.66E-07
Activated	MF	GO:0005125	cytokine activity	25/579	1.12E-07	2.23E-05	1.99E-05
Activated	MF	GO:0022848	acetylcholine-gated cation-selective channel activity	6/579	5.77E-06	0.000861	0.00077
Activated	KEGG	hsa04080	Neuroactive ligand-receptor interaction	37/248	4.95E-11	1.19E-08	1.12E-08
Activated	KEGG	hsa04060	Cytokine-cytokine receptor interaction	26/248	8.91E-07	0.000107	0.000101
Activated	KEGG	hsa04514	Cell adhesion molecules	17/248	5.05E-06	0.000406	0.000383
Activated	KEGG	hsa04657	IL-17 signaling pathway	10/248	0.000536	0.028495	0.026883
Inactivated	BP	GO:0006936	muscle contraction	43/411	2.74E-20	9.03E-17	8.04E-17
Inactivated	BP	GO:0003012	muscle system process	47/411	3.82E-19	6.3E-16	5.61E-16
Inactivated	BP	GO:0006939	smooth muscle contraction	17/411	3.45E-10	3.79E-07	3.37E-07
Inactivated	BP	GO:0035637	multicellular organismal signaling	19/411	3.47E-09	2.86E-06	2.54E-06
Inactivated	CC	GO:0043292	contractile fiber	36/445	1.49E-19	5.1E-17	3.83E-17
Inactivated	CC	GO:0030016	myofibril	33/445	2E-17	3.43E-15	2.58E-15
Inactivated	CC	GO:0030017	sarcomere	31/445	9.47E-17	1.08E-14	8.14E-15
Inactivated	CC	GO:0031674	I band	23/445	8.61E-14	7.39E-12	5.55E-12
Inactivated	MF	GO:0022836	gated channel activity	27/429	3.25E-08	1.01E-05	8.39E-06
Inactivated	MF	GO:0015267	channel activity	33/429	5.04E-08	1.01E-05	8.39E-06
Inactivated	MF	GO:0022803	passive transmembrane transporter activity	33/429	5.29E-08	1.01E-05	8.39E-06
Inactivated	MF	GO:0005261	cation channel activity	26/429	1.65E-07	2.1E-05	1.75E-05
Inactivated	KEGG	hsa00350	Tyrosine metabolism	10/208	1.32E-08	3.03E-06	2.45E-06
Inactivated	KEGG	hsa00982	Drug metabolism - cytochrome P450	13/208	2.47E-08	3.03E-06	2.45E-06
Inactivated	KEGG	hsa04020	Calcium signaling pathway	23/208	3.75E-08	3.07E-06	2.48E-06
Inactivated	KEGG	hsa04080	Neuroactive ligand-receptor interaction	28/208	1.21E-07	7.39E-06	5.97E-06

Table S4. Immune-related pathways associated with SLC7A5 expression enriched by GSEA analysis

Description	setSize	enrichmentScore	NES	*p* value	p.adjust	q value
Reactome_pd_1_signaling	21	0.788942	1.999073	2.02E-05	0.001301	0.001127
Wp_cancer_immunotherapy_by_pd1_blockade	23	0.750307	1.952202	9.42E-05	0.004196	0.003634
Wp_interactions_of_natural_killer_cells_in_pancreatic_cancer	28	0.731339	1.972684	6.03E-05	0.003041	0.002633
Pid_cd8_tcr_downstream_pathway	56	0.705812	2.19498	5.19E-08	2.6E-05	2.25E-05
Reactome_interleukin_10_signaling	45	0.703201	2.112873	9.76E-07	0.000164	0.000142
Kegg_hedgehog_signaling_pathway	55	0.672314	2.080325	6.08E-07	0.000127	0.00011
Kegg_antigen_processing_and_presentation	69	0.641981	2.080141	9.81E-07	0.000164	0.000142
Wp_tcell_receptor_signaling_pathway	88	0.576027	1.947667	3.37E-06	0.000423	0.000366
Kegg_natural_killer_cell_mediated_cytotoxicity	121	0.559083	1.977087	4.63E-07	0.00012	0.000104

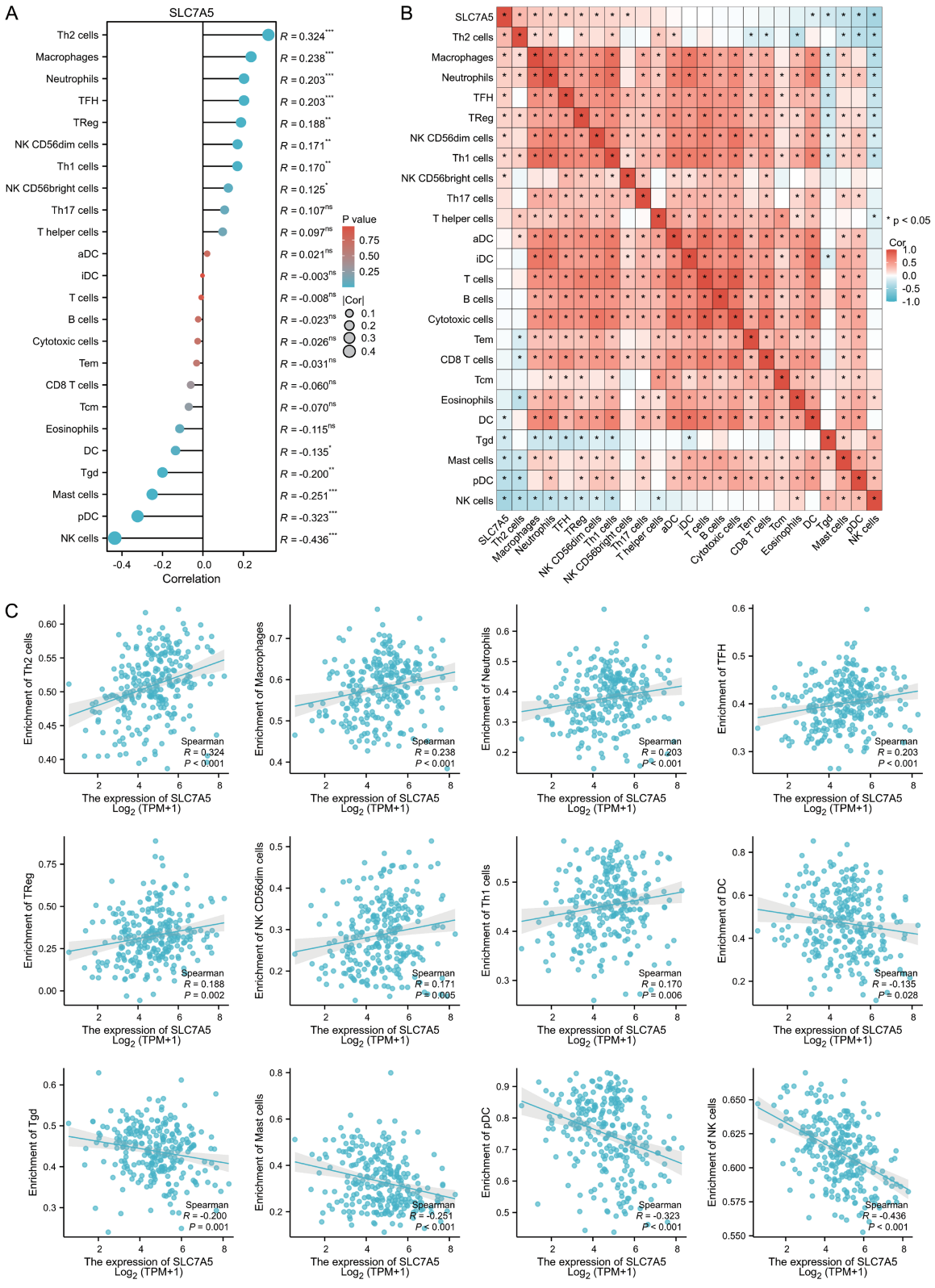

Figure S2. Correlation between SLC7A5 expression and immune cell infiltration. A. The lollipop graph shows the correlation between SLC7A5 and immune cell infiltration levels in sarcoma. B. Heatmap shows the correlation between SLC7A5 expression and Th2 cells, macrophages, neutrophils, TFH cells, Treg cells, NK CD56dim cells, Th1, NK cells, pDC cells, mast cells, Tgd cells, and DCs in sarcoma. C. Scatterplots of correlations between SLC7A5 expression and corresponding immune cells. SLC7A5, solute carrier family 7 member 5; TFH, Treg, regulatory T cells; Th, T helper; NK, natural killer; DC, dendritic cells; pDCs, plasmacytoid dendritic cells; TFH, T follicular helper; TGD, γδ T cells.

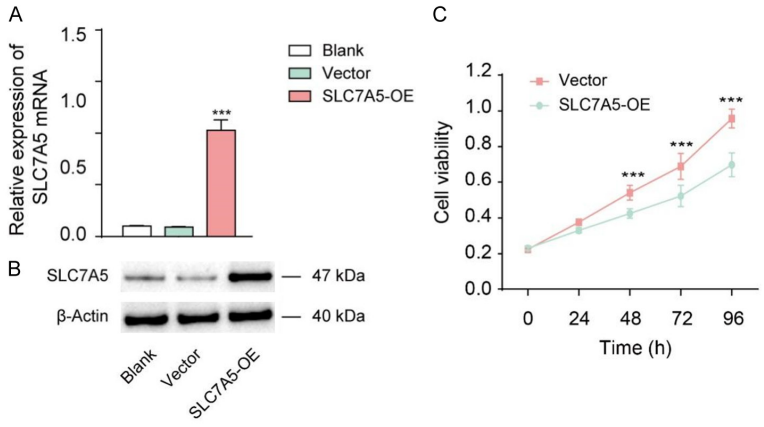

Figure S3. Effect of SLC7A5 overexpression on cell proliferation in MG63 cells. A. RT-qPCR validation of SLC7A5 mRNA levels after lentivirus-mediated overexpression in MG63 cells. B. Western blot analysis confirming elevated SLC7A5 protein expression following transfection. C. CCK-8 assay demonstrating the effect of SLC7A5 overexpression on cell proliferation. Data are presented as mean ± SD from three independent experiments (n = 3). ***P < 0.001 analyzed with Students' t-test. ####P < 0.0001 analyzed with repeated measures ANOVA.